LETTER

doi:10.1038/nature18956

A nucleosynthetic origin for the Earth's anomalous ^{142}Nd composition

C. Burkhardt[1,2], L. E. Borg[3], G. A. Brennecka[2,3], Q. R. Shollenberger[2,3], N. Dauphas[1] & T. Kleine[2]

A long-standing paradigm assumes that the chemical and isotopic compositions of many elements in the bulk silicate Earth are the same as in chondrites[1–4]. However, the accessible Earth has a greater ^{142}Nd/^{144}Nd ratio than do chondrites. Because ^{142}Nd is the decay product of the now-extinct ^{146}Sm (which has a half-life of 103 million years[5]), this ^{142}Nd difference seems to require a higher-than-chondritic Sm/Nd ratio for the accessible Earth. This must have been acquired during global silicate differentiation within the first 30 million years of Solar System formation[6] and implies the formation of a complementary ^{142}Nd-depleted reservoir that either is hidden in the deep Earth[6], or lost to space by impact erosion[3,7]. Whether this complementary reservoir existed, and whether or not it has been lost from Earth, is a matter of debate[3,8,9], and has implications for determining the bulk composition of Earth, its heat content and structure, as well as for constraining the modes and timescales of its geodynamical evolution[3,7,9,10]. Here we show that, compared with chondrites, Earth's precursor bodies were enriched in neodymium that was produced by the slow neutron capture process (s-process) of nucleosynthesis. This s-process excess leads to higher ^{142}Nd/^{144}Nd ratios; after correction for this effect, the ^{142}Nd/^{144}Nd ratios of chondrites and the accessible Earth are indistinguishable within five parts per million. The ^{142}Nd offset between the accessible silicate Earth and chondrites therefore reflects a higher proportion of s-process neodymium in the Earth, and not early differentiation processes. As such, our results obviate the need for hidden-reservoir or super-chondritic Earth models and imply a chondritic Sm/Nd ratio for the bulk Earth. Although chondrites formed at greater heliocentric distances and contain a different mix of presolar components than Earth, they nevertheless are suitable proxies for Earth's bulk chemical composition.

Coupled ^{146,147}Sm–^{142,143}Nd systematics is a powerful tool to constrain the timescales and processes involved in the early differentiation of Earth, the Moon and Mars[6,7,11–14]. However, the interpretation of ^{142}Nd signatures is complicated by the presence of nucleosynthetic isotope variations between the terrestrial planets and meteorites. Such isotope anomalies arise from the heterogeneous distribution of presolar matter at the planetary scale, and have been documented for several elements[15–18]. Because different Nd isotopes have varying contributions from the proton process (p-process), the rapid neutron capture process (r-process), and the s-process of stellar nucleosynthesis (Extended Data Fig. 1), the observed ^{142}Nd deficits in chondrites relative to the accessible Earth could, in principle, be nucleosynthetic in origin and hence unrelated to ^{146}Sm decay[8,16,19]. Previous studies have identified nucleosynthetic Nd (and Sm) isotope anomalies in

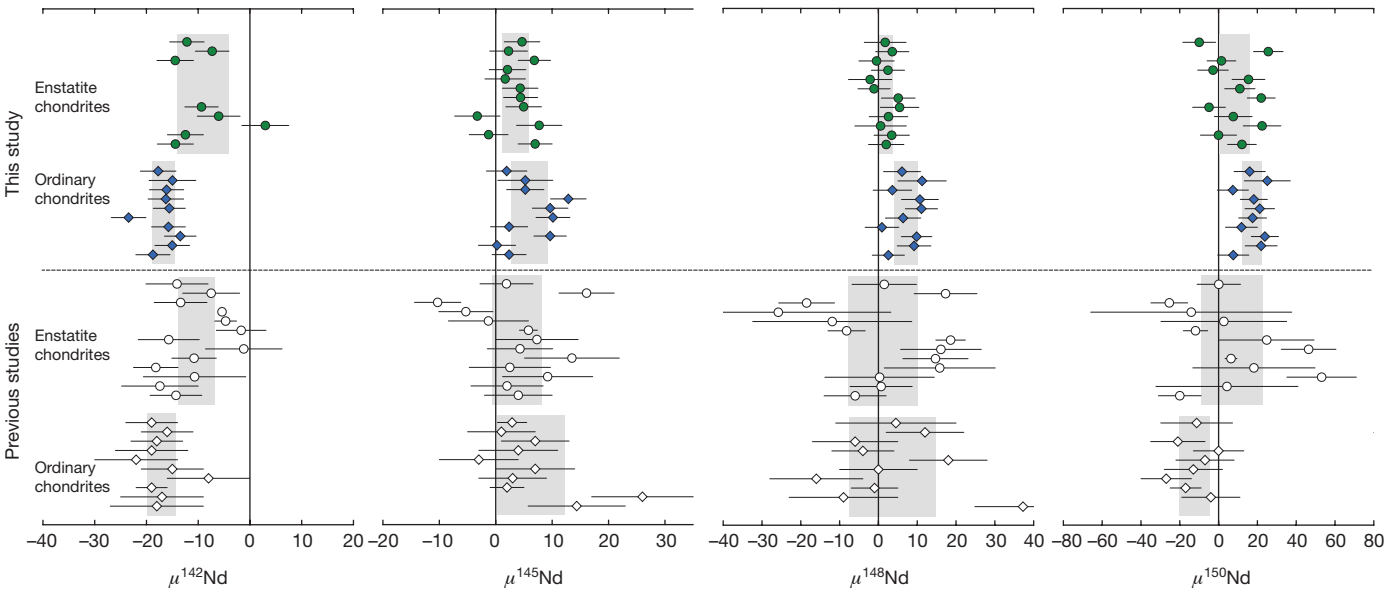

Figure 1 | Nd isotope compositions of enstatite and ordinary chondrites. Data from this study (solid symbols) show less scatter and more precisely defined mean values (the grey bars represent the 95% CI of the means from Student's *t*-values) than data from previous studies[6,15,17,24] (open symbols), and thus reveal systematic correlated anomalies in all Nd isotopes. The uncertainties shown for the individual data points are 2 standard errors (s.e. = standard deviation/$\sqrt{n}$; where n is the number of cycles per measurement) of the individual measurements. The origin of the different μ^{150}Nd values for the ordinary chondrites analysed in this study and previous studies is unclear. We note, however, that our processed standards are indistinguishable from the unprocessed JNdi-1 standard within the uncertainty, rendering it unlikely that an analytical effect in our study is responsible. Furthermore, our μ^{150}Nd data for ordinary chondrites are correlated with anomalies in other Nd isotopes, as expected.

[1]Origins Laboratory, Department of the Geophysical Sciences and Enrico Fermi Institute, The University of Chicago, 5734 South Ellis Avenue, Chicago, Illinois 60637, USA. [2]Institut für Planetologie, Westfälische Wilhelms-Universität Münster, Wilhelm Klemm-Strasse 10, 48149 Münster, Germany. [3]Lawrence Livermore National Laboratory, L231, Livermore, California 94550, USA.

Table 1 | Sm/Nd ratios and Nd and Sm isotope compositions of meteoritic and terrestrial samples

Sample	Type	$^{147}Sm/^{144}Nd$ measured	$\mu^{142}Nd$ measured	$\mu^{142}Nd$ corrected	$\mu^{145}Nd$	$\mu^{148}Nd$	$\mu^{150}Nd$	$\mu^{144}Sm$	$\mu^{148}Sm$	$\mu^{149}Sm$	$\mu^{150}Sm$	$\mu^{154}Sm$
Hvittis (1)	EL6	0.1999(2)	−6 (5)	−12 (5)	5 (9)	2 (5)	−10 (24)	6 (22)	1 (12)	−73 (14)	159 (12)	10 (18)
Hvittis (2)	EL6	0.1986(2)	−3 (6)	−7 (6)	2 (6)	4 (7)	26 (24)	−9 (43)	−1 (10)	−76 (10)	161 (18)	2 (13)
Hvittis (3)	EL6	0.1993(2)	−10 (8)	−14 (8)	7 (13)	0 (15)	1 (31)	0 (38)	4 (10)	−75 (12)	156 (13)	−7 (11)
Atlanta (1)	EL6	0.1909(2)	−5 (6)	3 (6)	2 (6)	2 (7)	−3 (24)	14 (43)	0 (10)	−44 (10)	101 (18)	12 (13)
Atlanta (2)	EL6	0.1849(2)	−8 (8)	8 (8)	2 (13)	−2 (15)	15 (31)	−10 (43)	0 (10)	−44 (10)	91 (18)	−7 (13)
Blithfield (1)	EL6	0.2285(2)	22 (6)	−26 (6)	4 (6)	−1 (7)	11 (24)	−2 (43)	3 (10)	−34 (10)	85 (18)	1 (13)
Blithfield (2)	EL6	0.1998(2)	−9 (8)	−14 (8)	4 (13)	5 (15)	22 (31)	14 (38)	0 (10)	−51 (12)	90 (13)	3 (11)
Saint Sauveur	EH6	0.1956(2)	−10 (5)	−9 (5)	5 (9)	5 (5)	−5 (24)	−17 (22)	−6 (12)	−49 (14)	104 (12)	−4 (18)
Abee (1)	EH4	0.1874(2)	−19 (6)	−6 (6)	−3 (6)	3 (7)	8 (24)	−18 (43)	−6 (10)	−39 (10)	80 (18)	−5 (13)
Abee (2)	EH4	0.1903(2)	−5 (8)	3 (8)	8 (13)	1 (15)	22 (31)	−15 (43)	0 (10)	−33 (10)	76 (18)	−4 (13)
Indarch (1)	EH4	0.1953(2)	−14 (6)	−12 (6)	−1 (6)	3 (7)	0 (24)	18 (43)	0 (10)	−35 (10)	85 (18)	3 (13)
Indarch (2)	EH4	0.1948(2)	−16 (8)	−14 (8)	7 (13)	2 (15)	12 (31)	−7 (43)	−5 (10)	−68 (10)	130 (18)	3 (13)
Average enstatite chondrites			**−10.4 (4.5)**	**−9.2 (4.9)**	**3.4 (2.1)**	**1.9 (1.5)**	**8.3 (7.4)**	**−2 (8)**	**−1 (2)**			**0 (4)**
Kernouve	H6	0.1926(2)						18 (22)	−1 (12)	10 (14)	−3 (12)	5 (18)
Queens Mercy	H6	0.1946(2)	−20 (5)	−18 (5)	2 (9)	6 (5)	16 (24)	11 (22)	−2 (12)	11 (14)	4 (12)	12 (18)
Allegan	H5	0.1952(2)	−16 (5)	−15 (5)	5 (9)	11 (6)	25 (24)	0 (22)	−8 (12)	−12 (14)	29 (12)	3 (18)
Forest City	H5	0.1944(2)	−19 (5)	−16 (5)	5 (9)	4 (6)	7 (24)	−4 (22)	−12 (12)	0 (14)	19 (12)	11 (18)
Pultusk	H5	0.1934(2)	−20 (8)	−16 (8)	13(13)	11 (15)	18 (31)	13 (38)	2 (10)	−52 (12)	93 (13)	−3 (11)
Sainte Marguerite (1)	H4	0.1955(2)	−16 (6)	−16 (6)	10 (6)	11 (7)	21 (24)	12 (43)	1 (10)	−16 (10)	39 (18)	1 (13)
Sainte Marguerite (2)	H4	0.1954(2)	−24 (8)	−23 (8)	10 (13)	6 (15)	18 (31)	0 (38)	−4 (10)	−18 (12)	34 (13)	−11 (11)
Bruderheim	L6	0.1935(2)	−19 (5)	−16 (5)	2 (9)	1 (5)	12 (24)	−4 (22)	2 (12)	−58 (14)	122 (12)	4 (18)
Farmington (1)	L5	0.1944(2)						26 (22)	−4 (12)	6 (14)	−1 (12)	−2 (18)
Farmington (2)	L5	0.1944(2)	−16 (6)	−13 (6)	10 (6)	10 (7)	24 (24)	−10 (43)	−2 (10)	9 (10)	6 (18)	−7 (13)
Dhurmsala	LL6	0.1965(2)	−14 (5)	−15 (5)	0 (9)	9 (5)	22 (24)	−12(22)	5 (12)	1 (14)	23 (12)	−12 (18)
Paragould	LL5	0.1924(2)						22 (22)	−5 (12)	−70 (14)	133 (12)	2 (18)
Chelyabinsk	LL5	0.1963(2)	−18 (5)	−19 (5)	2 (9)	3 (4)	8 (24)	3 (22)	1 (12)	−8 (14)	20 (12)	4 (18)
Average ordinary chondrites			**−18.3 (2.1)**	**−16.7 (2.0)**	**6.0 (3.1)**	**7.2 (2.7)**	**17.0 (4.6)**	**6 (7)**	**−2 (3)**			**1 (4)**
Allende (1)	CV3	0.1929(2)						−85 (22)	−2 (12)	−46 (14)	97 (12)	−7 (18)
Allende (2)	CV3	0.1959(2)	−30 (5)	−30 (5)	2 (9)	9 (4)	8 (24)	−68 (22)	−8 (12)	−31 (14)	73 (12)	−2 (18)
Allende (3)	CV3	0.1961(2)	−30 (6)	−31 (6)	5 (6)	4 (7)	−6 (24)	−77 (22)	−8 (12)	−33 (14)	73 (12)	−1 (18)
Allende (4)	CV3	0.1948(2)	−33 (8)	−31 (8)	8 (13)	16 (15)	11 (31)	−89 (38)	4 (10)	−29 (12)	79 (13)	−19 (11)
Average CV			**−31.3 (3.7)**	**−30.7 (1.1)**	**5.2 (7.5)**	**9 (16)**	**4 (22)**	**−80 (15)**	**−3 (9)**			**−7 (13)**
NWA 5363	Ung.	0.2520(2)	**67.1(5.9)**	**−16.0 (7.5)**	**11 (6)**	**17.1 (7.3)**	**39 (24)**	**27 (43)**	**−1 (10)**	**−109 (10)**	**211 (18)**	**−4 (13)**
A−ZH-5	CAI	0.2000(12)	**−9.2 (7.6)**	**−15.2 (7.8)**	**−19 (13)**	**−28 (15)**	**−47 (31)**	**−233 (38)**	**62 (10)**	**−35 (12)**	**121 (13)**	**−43 (11)**
JNdi-1 (1)	Std		0 (5)	0 (5)	−6 (9)	−5 (5)	−2 (24)					
BHVO-2	Std	0.1484(2)	−1 (5)	−1 (5)	−2 (9)	−7 (5)	−3 (24)	−7 (22)	4 (12)	6 (14)	7 (12)	−6 (18)
JNdi-1 (2)	Std		0 (8)	0 (8)	0 (13)	0 (15)	0 (31)					
BIR-1	Std	0.2759(3)	−2 (8)	−2 (8)	5 (13)	0 (15)	−10 (31)	−10 (38)	7 (10)	1 (12)	4 (13)	−17 (11)
Average of the processed standards			**−0.5 (1.6)**	**−0.5 (1.6)**	**−0.7 (7.2)**	**−3.0 (5.6)**	**−3.8 (7.3)**	**−9 (19)**	**5 (12)**	**4 (14)**	**5 (18)**	**−11 (18)**

$\mu^i Nd = [(^iNd/^{144}Nd)_{sample}/(^iNd/^{144}Nd)_{standard} - 1] \times 10^6$ and $\mu^i Sm = [(^iSm/^{152}Sm)_{sample}/(^iSm/^{152}Sm)_{standard} - 1] \times 10^6$, where all ratios have been corrected for mass fractionation by internal normalizations to fixed $^{146}Nd/^{144}Nd$ and $^{147}Sm/^{152}Sm$ ratios using the exponential law. 'μ^{142}Nd corrected' denotes μ^{142}Nd corrected for radiogenic ^{142}Nd variations to a common chondritic value ($^{147}Sm/^{144}Nd = 0.1960$). Individual sample data represent the average values of up to five measurement runs from the same filament (the full data set is available in Supplementary Information). Repeat samples (denoted 1–4) represent separate digestions that were processed though chemistry at different times and run on separate filaments. The uncertainties shown in parentheses are the external reproducibilities of the standard (2 s.d.) or two-sided Student's *t*-values 95% confidence intervals (for group averages with $n > 2$). The deficits in μ^{149}Sm values and excesses in μ^{150}Sm values that are present in some meteorite samples are due to thermal neutron capture reactions of ^{149}Sm during exposure to galactic cosmic rays, so group averages are not reported (Extended Data Fig. 5). CV refers to the Vigerano-like group of chondrites. Samples and group averages displayed in Figs 2 and 3 are in bold. Ung., ungrouped achondrite.

chondrites[15,17] and their components[20–23], but these effects do not seem to fully account for the observed ^{142}Nd deficits in chondrites. For instance, although the ^{142}Nd composition of carbonaceous chondrites can partly be attributed to s- or p-process deficits[15,17], corrections for these effects still leave an ^{142}Nd deficit of approximately 20 p.p.m. compared with the accessible silicate Earth. This would be consistent with Nd isotope data for bulk ordinary chondrites, which exhibit a deficit of a similar magnitude, but do not seem to show resolvable

nucleosynthetic Nd isotope anomalies[15,17,24]. Enstatite chondrites have ^{142}Nd deficits of approximately 10 p.p.m. and also do not show clearly resolved nucleosynthetic Nd isotope anomalies[24]. Thus, previous studies concluded that the ^{142}Nd difference between chondrites and the accessible Earth largely reflects ^{146}Sm decay and early Sm/Nd fractionation in the silicate Earth[15,17,24]. However, this interpretation remains uncertain because the available bulk chondrite data are of insufficient precision to detect the collateral effects of nucleosynthetic heterogeneities on non-radiogenic Nd isotopes and therefore do not permit the reliable quantification of nucleosynthetic ^{142}Nd variations (Fig. 1).

Here we use high-precision Nd and Sm isotope measurements to better quantify the nucleosynthetic Nd isotope variations between chondrites and the Earth, with the ultimate goal of determining the magnitude of any radiogenic ^{142}Nd difference. We digested larger sample sizes (around 2 g) than in most previous studies, allowing us to obtain higher-precision Nd and Sm isotope data for a comprehensive set of meteorites that includes 18 chondrites, the ungrouped brachinite-like achondrite NWA 5363 and the Ca–Al-rich inclusion (CAI) A-ZH-5 from the Allende chondrite (Table 1). To evaluate the accuracy of our data we also processed the JNdi-1 standard and the terrestrial basalts BHVO-2 and BIR-1 using the same analytical procedures. Within uncertainty, the Nd and Sm isotope compositions of the processed and unprocessed standards (JNdi-1, AMES) are indistinguishable (Table 1; Figs 2, 3).

Most of the chondrites investigated cluster tightly around a ^{147}Sm–^{143}Nd isochron at 4.568 billion years ago (Ga) (Extended Data Fig. 2a). Only the EL6 chondrites Atlanta and Blithfield plot away from the isochron, probably reflecting disturbance by late-stage impact events[25]; the ^{142}Nd data of these samples are therefore excluded from the following discussion. After correction of measured μ^{142}Nd (for definition of μ^{i}Nd and μ^{i}Sm see Table 1) values for ^{146}Sm decay to the average chondritic ^{147}Sm/^{144}Nd = 0.1960 (ref. 1; Extended Data Table 1), the μ^{142}Nd values are tightly clustered for each chondrite group: the enstatite chondrites define a mean $\mu^{142}\text{Nd} = -9 \pm 5$ (95% confidence interval; CI), the ordinary chondrites a mean $\mu^{142}\text{Nd} = -17 \pm 2$ (95% CI) and the Allende CV3 chondrite a mean $\mu^{142}\text{Nd} = -31 \pm 1$ (95% CI). NWA 5363 exhibits a decay-corrected μ^{142}Nd of -16 ± 7, similar to ordinary chondrites, whereas CAI A-ZH-5 has a decay-corrected μ^{142}Nd of -15 ± 8, consistent with the data for other Allende CAIs[22].

In addition to variations in μ^{142}Nd, we find resolved systematic variations in non-radiogenic Sm and Nd isotopes (Table 1, Figs 1–3). Compared with previous studies we observe less scatter for each chondrite group, reflecting the long duration and high beam intensity of our measurements, which result in more precisely defined average values for each group (Fig. 1). Plots of μ^{145}Nd and μ^{150}Nd versus μ^{148}Nd reveal positively correlated anomalies, with the enstatite chondrites being closest to the terrestrial value, followed by carbonaceous and ordinary chondrites, and then NWA 5363 (Fig. 2a, b). The meteorite samples plot along mixing lines between terrestrial Nd (that is, $\mu^{i}\text{Nd} = 0$) and pure s-process Nd, regardless of whether the s-process composition is derived from presolar SiC grains[26], nucleosynthesis models[27] or data for acid leachates of primitive chondrites[20,21]. Thus, the variability in non-radiogenic Nd isotopes among the meteorites reflects variable s-deficits relative to the Earth, consistent with inferences from other elements[16,28,29].

The μ^{145}Nd, μ^{148}Nd and μ^{150}Nd anomalies of Allende are similar to those of ordinary and enstatite chondrites, although for most other elements nucleosynthetic anomalies are typically largest in carbonaceous chondrites[16,18,28–30]. The reason for the subdued Nd isotopic anomalies in Allende is the presence of CAIs, which host about half of the Nd and Sm in Allende[31], and which, for these elements, are characterized by an s-excess and a p-deficit (Figs 2, 3). Mass balance calculations (see Methods and Extended Data Table 2) indicate that the composition of a CAI-free Allende would have μ^{145}Nd, μ^{148}Nd and μ^{150}Nd values of 27 ± 14, 39 ± 28, and 56 ± 41, respectively; these anomalies are larger than those of ordinary and enstatite chondrites and thus imply that before addition of CAIs, the Allende chondrite

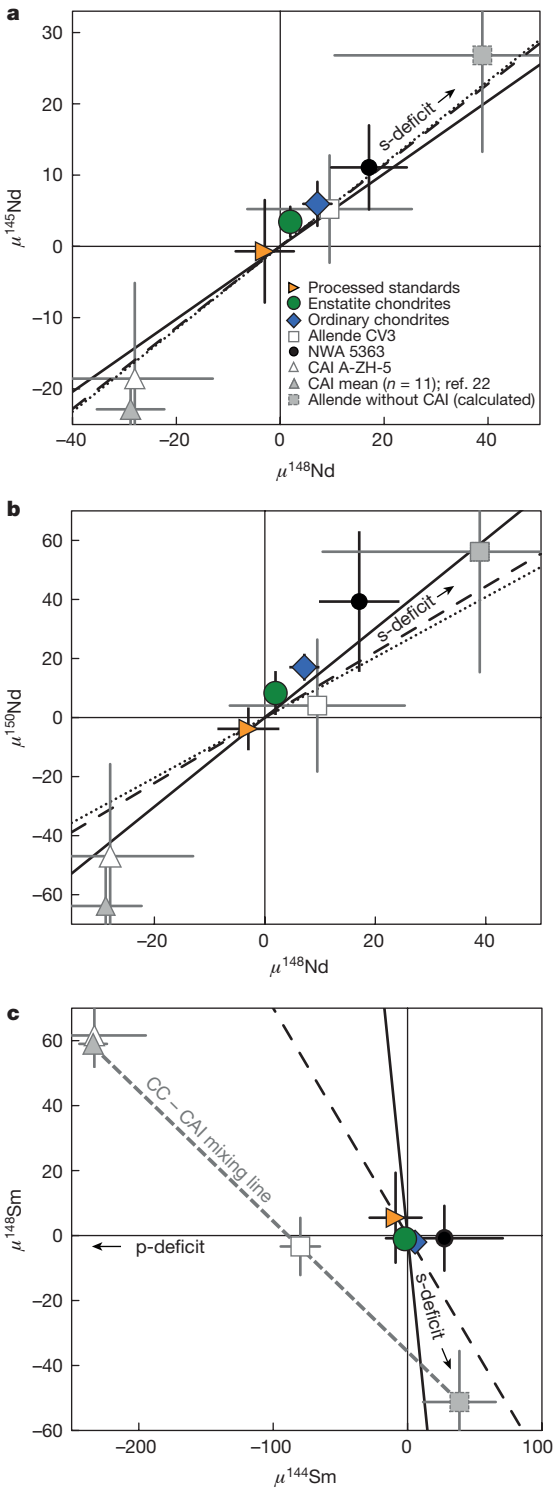

Figure 2 | Nd and Sm isotope variations among meteoritic and terrestrial samples. a, Anomalies in non-radiogenic Nd isotopes μ^{145}Nd and μ^{148}Nd are consistent with a heterogeneous distribution of s-process Nd. Solid, dotted and dashed lines are the mixing lines between terrestrial Nd and s-process Nd, calculated using modelled s-process compositions[27], Nd data for presolar SiC grains[26] and Nd data for chondrite leachates[20,21], respectively. The isotopic composition measured for bulk Allende can be accounted for by the admixture of CAIs in a CAI-free carbonaceous chondrite (CC) source reservoir (the 'Allende without CAI (calculated)' data point) that is characterized by an s-process deficit. **b**, Same as **a** but for μ^{148}Nd and μ^{150}Nd. **c**, The p-deficit observed for bulk Allende in μ^{144}Sm can also be attributed to the admixture of CAIs. The grey dashed CC − CAI line represents a mixing line calculated by subtracting CAIs from the isotopic composition measured for bulk Allende. Error bars indicate the 95% CI.

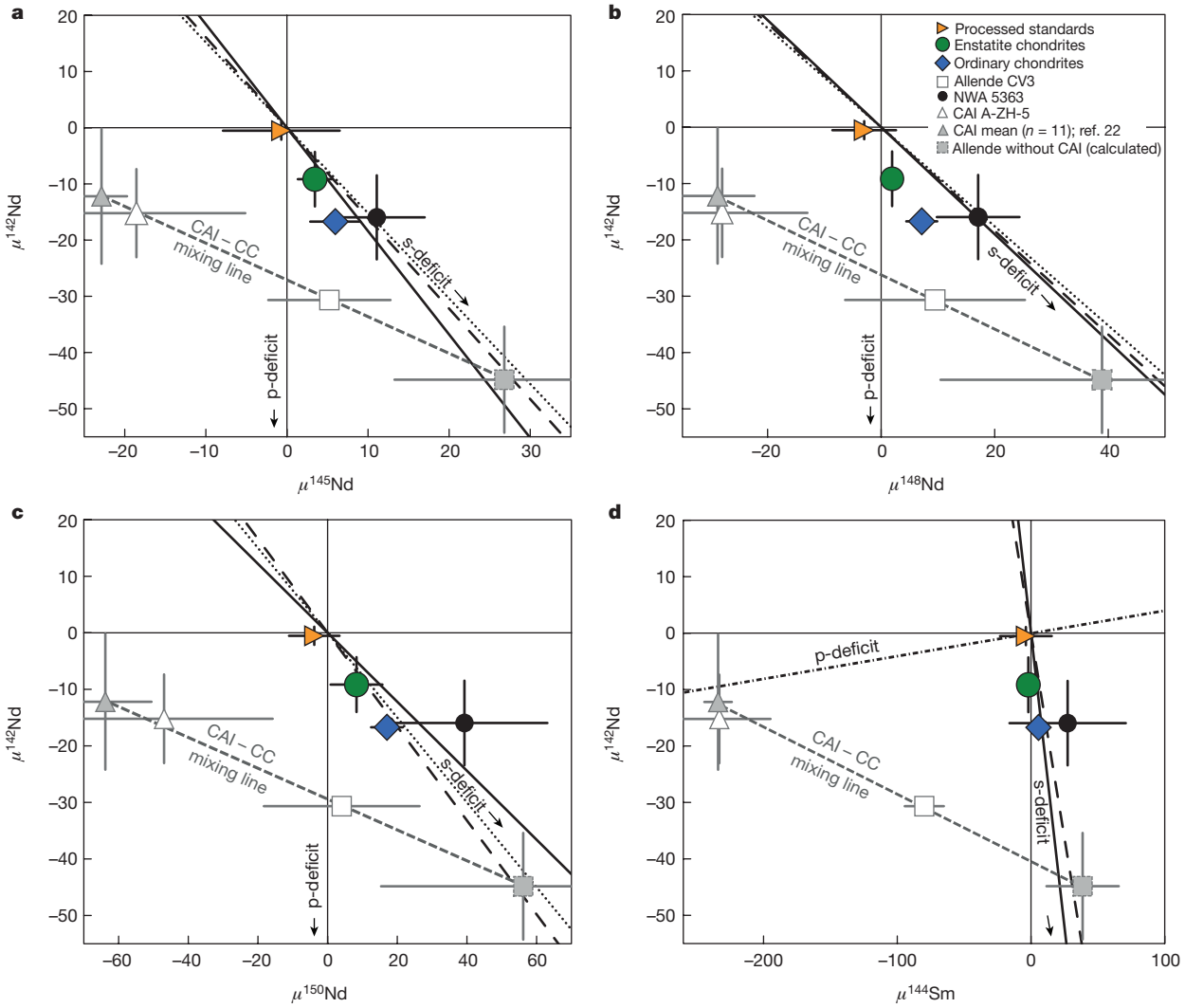

Figure 3 | Nd and Sm isotope variations among meteoritic and terrestrial samples. a, For enstatite chondrites, ordinary chondrites and NWA 5363, the μ^{142}Nd anomalies are correlated with the non-radiogenic μ^{145}Nd anomalies, as expected for a heterogeneous distribution of s-process Nd. The Allende carbonaceous chondrite plots off this correlation owing to the admixture of CAIs. Mass balance calculations indicate that a CAI-free carbonaceous chondrite source reservoir was characterized by an s-process deficit. **b**, Same as **a** but in μ^{142}Nd versus μ^{148}Nd space. **c**, Same as **a** but in μ^{142}Nd versus μ^{150}Nd space. **d**, Same as **a** but in μ^{142}Nd versus μ^{144}Sm space. Error bars indicate the 95% CI.

had a substantial s-deficit (Fig. 2a, b). This interpretation is consistent with Sm isotope data for Allende and other carbonaceous chondrites, because the calculated CAI-free composition of these chondrites also shows an s-deficit (Fig. 2c, Extended Data Fig. 3). Thus, the displacement of the carbonaceous chondrites from the s-deficit line that is defined by ordinary and enstatite chondrites reflects the admixture of CAIs to carbonaceous chondrites. Note that, for ordinary and enstatite chondrites the effects of admixing CAIs are estimated to be no larger than 2 p.p.m. for Nd isotope ratios and 5 p.p.m. for Sm isotope ratios (Methods, Extended Data Table 2), and that the expected s-process Sm isotope anomalies ($<10\mu^{144}$Sm and $>-20\mu^{148}$Sm) for these two groups of chondrites are too small to be resolvable with the analytical precision of our Sm isotope measurements.

Using the information gained from the non-radiogenic isotopes, we can now assess the effect of nucleosynthetic anomalies on μ^{142}Nd. The bulk meteorite data show inverse correlations between μ^{142}Nd and μ^{145}Nd, μ^{148}Nd, μ^{150}Nd and μ^{144}Sm (Fig. 3), which are consistent with the covariations expected from a heterogeneous distribution of s-process isotopes. Enstatite and ordinary chondrites, as well as NWA 5363, plot on mixing lines between terrestrial and s-process Nd. The Allende CV3 chondrite is displaced from these correlations owing to the admixture of CAIs, and a calculated CAI-free carbonaceous chondrite composition plots on the s-mixing line defined by the other meteorites (Fig. 3).

The slopes obtained from linear regressions of the bulk meteorites (excluding Allende) are in good agreement with those calculated for mixing lines between terrestrial and s-process Nd, regardless of which estimate for the s-process composition is used[20,21,26,27] and whether or not the calculated CAI-free carbonaceous chondrite composition and the processed standards are included in the regressions (Extended Data Fig. 4). The intercept values obtained from the regressions can thus be used to determine μ^{142}Nd values corrected for s-process heterogeneity. For all regressions the intercept values are indistinguishable from each other, with an average value of approximately −5 p.p.m. relative to the JNdi-1 standard (Extended Data Table 3). Alternatively, μ^{142}Nd values corrected for nucleosynthetic anomalies can be calculated for each meteorite group separately, using their measured μ^{145}Nd, μ^{148}Nd and μ^{150}Nd values combined with the slopes of the s-mixing lines. Regardless of which s-process mixing relationships are applied, the calculated $\mu^{142}Nd_{s\text{-corrected}}$ values are all mutually consistent and indistinguishable from each other (Extended Data Table 3), resulting in an average $\mu^{142}Nd_{s\text{-corrected}} = -5 \pm 2$ p.p.m. Although this value is slightly negative, it is within the approximate long-term ±5 p.p.m. reproducibility of the JNdi-1 standard. When the regressions and corrections are calculated relative to the mean Nd isotope composition measured for the processed terrestrial standards, $\mu^{142}Nd_{s\text{-corrected}}$ reduces to -2 ± 2 p.p.m. (Extended Data Table 3). We conclude that

after correction for nucleosynthetic Nd isotope heterogeneity, the ^{142}Nd compositions of chondrites and the accessible silicate Earth are indistinguishable at the current level of analytical precision (approximately 5 p.p.m.).

The lack of a resolved radiogenic ^{142}Nd difference between chondrites and the accessible silicate Earth supports the long-standing paradigm of a chondritic Sm/Nd for the bulk Earth and requires the revision of the conclusions from several previous studies about the early differentiation, composition, structure and heat budget of the Earth. These studies interpreted the ^{142}Nd offset between chondrites and terrestrial samples as resulting from ^{146}Sm-decay and an early global Sm/Nd fractionation in the Earth's mantle[3,6,7,9,10]. Our results instead demonstrate that chondrites and the accessible Earth have indistinguishable radiogenic ^{142}Nd compositions, refuting the evidence for an early global silicate differentiation of the Earth and indicating that the hidden, enriched reservoir hypothesized in earlier studies[3,6,9,10] does not exist. Moreover, our results rule out the extensive loss of early-formed crust by collisional erosion[3,7,9], because otherwise the bulk silicate Earth would not have a chondritic Sm/Nd ratio. Finally, the evidence for chondritic Sm/Nd ratios in the bulk Earth implies chondritic abundances of other refractory elements, including the heat-producing elements U and Th. Thus, the total radiogenic heat generated over Earth's history is almost a factor of two higher than was estimated recently for a non-chondritic composition of the Earth[9].

Our results demonstrate that chondrites are the most appropriate proxy for the elemental composition of the Earth. However, they also highlight that chondrites cannot be the actual building blocks of the Earth because they are deficient in a presolar component that contains s-process matter. The s-process deficit increases from enstatite via ordinary to carbonaceous chondrites, indicating that the distribution of presolar matter in the solar protoplanetary disk either varied as a function of heliocentric distance or over time. For instance, the nucleosynthetic isotope heterogeneity within the disk may reflect differences in the thermal processing of stellar-derived dust, imparting isotopic heterogeneity on an initially homogeneous disk, but it could also reflect distinct compositions of material added to the disk from the molecular cloud at different times[18,28–30]. Either way, the increasing deficit in s-process matter with increasing heliocentric distance provides a new means for identifying genetic relationships among planetary bodies. For instance, Mars formed at a greater heliocentric distance than Earth and should, therefore, be characterized by an s-process deficit that may be similar to those observed for enstatite and ordinary chondrites. Thus, high-precision Nd isotopic data for Martian meteorites will make it possible to determine the distinct sources of the building materials of Earth and Mars. This information is not only critical for dating the differentiation of Mars[13], but also for testing models of terrestrial planet formation.

Online Content Methods, along with any additional Extended Data display items and Source Data, are available in the online version of the paper; references unique to these sections appear only in the online paper.

Received 20 January; accepted 3 June 2016.

1. Bouvier, A., Vervoort, J. D. & Patchett, P. J. The Lu–Hf and Sm–Nd isotopic composition of CHUR: constraints from unequilibrated chondrites and implications for the bulk composition of terrestrial planets. *Earth Planet. Sci. Lett.* **273,** 48–57 (2008).
2. Nakamura, N. Determination of REE, Ba, Fe, Mg, Na, and K in carbonaceous and ordinary chondrites. *Geochim. Cosmochim. Acta* **38,** 757–775 (1974).
3. Campbell, I. H. & O'Neill, H. S. C. Evidence against a chondritic Earth. *Nature* **483,** 553–558 (2012).
4. Jacobsen, S. B. & Wasserburg, G. J. Sm–Nd isotopic evolution of chondrites. *Earth Planet. Sci. Lett.* **50,** 139–155 (1980).
5. Meissner, F., Schmidt-Ott, W.-D. & Ziegeler, L. Half-life and α-ray energy of ^{146}Sm. *Z. Phys. A* **327,** 171–174 (1987).
6. Boyet, M. & Carlson, R. W. ^{142}Nd evidence for early (>4.53 Ga) global differentiation of the silicate Earth. *Science* **309,** 576–581 (2005).
7. Caro, G., Bourdon, B., Halliday, A. & Quitté, G. Superchondritic Sm/Nd in Mars, Earth and the Moon. *Nature* **452,** 336–339 (2008).
8. Huang, S., Jacobsen, S. B. & Mukhopadhyay, S. ^{147}Sm–^{143}Nd systematics of Earth are inconsistent with a superchondritic Sm/Nd ratio. *Proc. Natl Acad. Sci. USA* **110,** 4929–4934 (2013).
9. Jellinek, A. M. & Jackson, M. G. Connections between the bulk composition, geodynamics and habitability of Earth. *Nat. Geosci.* **8,** 587–593 (2015).
10. Carlson, R. W. & Boyet, M. Composition of the Earth's interior: the importance of early events. *Phil. Trans. R. Soc. A* **366,** 4077–4103 (2008).
11. Bennett, V. C., Brandon, A. D. & Nutman, A. P. Coupled ^{142}Nd–^{143}Nd isotopic evidence for Hadean mantle dynamics. *Science* **318,** 1907–1910 (2007).
12. Brandon, A. D. *et al.* Re-evaluating ^{142}Nd/^{144}Nd in lunar mare basalts with implications for the early evolution and bulk Sm/Nd of the Moon. *Geochim. Cosmochim. Acta* **73,** 6421–6445 (2009).
13. Debaille, V., Brandon, A. D., Yin, Q. Z. & Jacobsen, B. Coupled ^{142}Nd–^{143}Nd evidence for a protracted magma ocean in Mars. *Nature* **450,** 525–528 (2007).
14. Harper, C. L. & Jacobsen, S. B. Evidence from coupled ^{147}Sm–^{143}Nd and ^{146}Sm–^{142}Nd systematics for very early (4.5 Gyr) differentiation of the Earth's mantle. *Nature* **360,** 728–732 (1992).
15. Andreasen, R. & Sharma, M. Solar nebula heterogeneity in p-process samarium and neodymium isotopes. *Science* **314,** 806–809 (2006).
16. Burkhardt, C. *et al.* Molybdenum isotope anomalies in meteorites: Constraints on solar nebula evolution and origin of the Earth. *Earth Planet. Sci. Lett.* **312,** 390–400 (2011).
17. Carlson, R. W., Boyet, M. & Horan, M. F. Chondrite barium, neodymium, and samarium isotopic heterogeneity and early Earth differentiation. *Science* **316,** 1175–1178 (2007).
18. Trinquier, A. *et al.* Origin of nucleosynthetic isotope heterogeneity in the solar protoplanetary disk. *Science* **324,** 374–376 (2009).
19. Sprung, P., Kleine, T. & Scherer, E. E. Isotopic evidence for chondritic Lu/Hf and Sm/Nd of the Moon. *Earth Planet. Sci. Lett.* **380,** 77–87 (2013).
20. Boyet, M. & Gannoun, A. Nucleosynthetic Nd isotope anomalies in primitive enstatite chondrites. *Geochim. Cosmochim. Acta* **121,** 652–666 (2013).
21. Qin, L. P., Carlson, R. W. & Alexander, C. M. O. Correlated nucleosynthetic isotopic variability in Cr, Sr, Ba, Sm, Nd and Hf in Murchison and QUE 97008. *Geochim. Cosmochim. Acta* **75,** 7806–7828 (2011).
22. Brennecka, G. A., Borg, L. E. & Wadhwa, M. Evidence for supernova injection into the solar nebula and the decoupling of *r*-process nucleosynthesis. *Proc. Natl Acad. Sci. USA* **110,** 17241–17246 (2013).
23. Marks, N. E., Borg, L. E., Hutcheon, I. D., Jacobsen, B. & Clayton, R. N. Samarium–neodymium chronology and rubidium–strontium systematics of an Allende calcium–aluminum-rich inclusion with implications for ^{146}Sm half-life. *Earth Planet. Sci. Lett.* **405,** 15–24 (2014).
24. Gannoun, A., Boyet, M., Rizo, H. & El Goresy, A. ^{146}Sm–^{142}Nd systematics measured in enstatite chondrites reveals a heterogeneous distribution of ^{142}Nd in the solar nebula. *Proc. Natl Acad. Sci. USA* **108,** 7693–7697 (2011).
25. Rubin, A. E. Impact features of enstatite-rich meteorites. *Chem. Erde-Geochem.* **75,** 1–28, (2015).
26. Hoppe, P. & Ott, U. Mainstream silicon carbide grains from meteorites. *AIP Conf. Proc.* **402,** 27–58 (1997).
27. Arlandini, C., Käppeler, F. & Wisshak, K. Neutron capture in low-mass asymptotic giant branch stars: cross sections and abundance signatures. *Astrophys. J.* **525,** 886–900 (1999).
28. Akram, W., Schönbächler, M., Bisterzo, S. & Gallino, R. Zirconium isotope evidence for the heterogeneous distribution of s-process materials in the solar system. *Geochim. Cosmochim. Acta* **165,** 484–500 (2015).
29. Fischer-Gödde, M., Burkhardt, C., Kruijer, T. S. & Kleine, T. Ru isotope heterogeneity in the solar protoplanetary disk. *Geochim. Cosmochim. Acta* **168,** 151–171 (2015).
30. Dauphas, N. *et al.* Calcium-48 isotopic anomalies in bulk chondrites and achondrites: evidence for a uniform isotopic reservoir in the inner protoplanetary disk. *Earth Planet. Sci. Lett.* **407,** 96–108 (2014).
31. Stracke, A. *et al.* Refractory element fractionation in the Allende meteorite: implications for solar nebula condensation and the chondritic composition of planetary bodies. *Geochim. Cosmochim. Acta* **85,** 114–141 (2012).

Supplementary Information is available in the online version of the paper.

Acknowledgements We thank the Field Museum for providing samples, S.-G. Lee for help setting up the chemistry in Chicago, R. Carlson for discussions. This work was funded through SNF PBE2PZ-145946 (CB); NASA (NNX14AK09G, OJ-30381-0036A, NNX15AJ25G), NSF (EAR144495, EAR150259) (ND); NASA NNH12AT84I (LB) and the ERC (Grant Agreement 616564 'ISOCORE') (TK). The work performed by L.E.B., G.A.B., and Q.R.S. was done under the auspices of the US Department of Energy by Lawrence Livermore National Laboratory under Contract DE-AC52-07NA27344.

Author Contributions C.B. initiated the project in collaboration with L.E.B., N.D. and T.K., acquired and processed the samples in Chicago and wrote a first draft of the manuscript. L.E.B., G.A.B. and Q.R.S. performed additional chemistry and measured all samples in Livermore. All authors contributed to the data interpretation and editing of the manuscript.

Author Information Data are available at the EarthChem library (http://dx.doi.org/10.1594/IEDA/100597). Reprints and permissions information is available at www.nature.com/reprints. The authors declare no competing financial interests. Readers are welcome to comment on the online version of the paper. Correspondence and requests for materials should be addressed to C.B. (burkhardt@uni-muenster.de).

METHODS

Samples. To avoid the artefacts that can be associated with incomplete dissolution of refractory presolar components and to minimize potential disturbances through terrestrial alteration, only equilibrated chondrites (petrologic classes 4–6; except the CV3 Allende) from observed falls were selected for this study. Equilibrated chondrites are devoid of presolar grains because these components were destroyed during thermal metamorphism on the meteorite parent body[32]; for Allende (metamorphic grade of 3.2 to >3.6), which may contain trace amounts of presolar grains[32], no difference in Nd isotopic composition was observed between table-top acid-digested, bomb-digested and alkali-fused samples[6,17], indicating that for this meteorite all Nd carriers are accessed by standard acid digestion. Our sample set includes eleven ordinary chondrites (six H, two L and three LL), six enstatite chondrites (three EL and three EH), the carbonaceous chondrite Allende and the brachinite-like achondrite NWA 5363, which is a melt-depleted ultramafic sample from a partially differentiated asteroid[33]. This brachinite-like sample was added to the study because of its unique isotope anomalies: while the oxygen and nickel isotopic compositions of NWA 5363 are indistinguishable from terrestrial values, it exhibits nucleosynthetic isotope anomalies in Ti, Ca, Mo and Ru that are closer to ordinary chondrites[34]. In addition to bulk meteorites, we analysed the CAI A-ZH-5 from the Allende chondrite and, to evaluate the accuracy of our analytical methods, we also processed the JNdi-1 standard, as well as the terrestrial basalt standards BHVO-2 and BIR-1.

Sample preparation and chemical separation of Nd and Sm. Meteorite pieces were cleaned with abrasive paper, ultrasonicated in methanol and subsequently crushed to a fine powder in an acid-cleaned agate mortar exclusively used for meteorite work at the Origins Laboratory, Chicago. For each analysis about 2 g of meteorite powder was digested in a HF–HNO_3–$HClO_4$ mixture and aqua regia in 90 ml Savillex teflon vials for about 10 d on a hotplate at 170 °C. After several dry-downs, ultrasonication and redissolution steps in aqua regia and HCl, the samples were redissolved in HCl and, once a clear solution was obtained, an aliquot of approximately 5% was taken for Sm and Nd concentration measurements by isotope dilution.

Chemical procedures for Sm and Nd concentration measurements. The 5% aliquots were sent from the Origins Laboratory to the Lawrence Livermore National Laboratory (LLNL), where they were equilibrated with a ^{149}Sm–^{150}Nd mixed isotopic tracer. Rare earth elements (REE) were purified from the matrix of these aliquots using 2 ml BioRad columns filled with AG50-X8 (200–400 mesh) resin and 2 M and 6 M HCl. The REE were further purified using 150 µl Teflon columns with RE-Spec resin and 1 M and 0.05 M HNO_3. Sm and Nd were purified from the other REE using 15 cm glass columns, Ln-Spec resin and 0.25 M and 0.60 M HCl. Total blanks of the isotope dilution procedures were 25 pg of Nd and 8 pg of Sm, resulting in Nd and Sm sample-to-blank ratios greater than 1,500 for all but one sample. The blank corrections resulted in shifts in the $^{147}Sm/^{144}Nd$ ratios that were less than 0.003% and thus substantially smaller than the typical uncertainty of 0.1% associated with the isotope dilution measurements. For NWA 5363, the Nd and Sm sample-to-blank ratios were 751 and 760, respectively, and thus required a blank correction of 0.13% for the Nd and Sm concentrations (for example, the reported 0.112 p.p.m. Nd abundance was corrected by 0.00015 p.p.m.). The blank correction is reflected in the larger uncertainty of 0.2% on the $^{147}Sm/^{144}Nd$ of NWA 5363.

Chemical procedures for Sm and Nd isotope composition measurements. After aliquoting, the remaining 95% of the sample solution was reduced and HNO_3 was added. The REE cut of CAI A-ZH-5 that was obtained in a previous study[35] (where the digested sample was processed through an anion exchange chromatography to separate Ti, Zr, Hf, W and Mo from the matrix; for details see ref. 35) was added to the project at this point. After additional dry-downs in aqua regia and HNO_3, samples were redissolved in approximately 35 ml of 3 M HNO_3 and 350 mg of H_3BO_3 was added before the solutions were centrifuged. A fine-grained, black, low-density residue (probably carbon-based) was present for some of the chondrites at this point and was discarded; note that because we analysed equilibrated chondrites, this C-bearing phase does not contain presolar material and therefore does not influence the Nd isotopic composition of the non-radiogenic isotopes. Furthermore, changes in the Sm/Nd ratios or the radiogenic Nd isotopic signatures of the samples by this material is also excluded, given the very good agreement of our decay-corrected ^{142}Nd and ^{143}Nd data with previous studies (Fig. 1; Extended Data Fig. 2). After centrifugation, the REE were separated from the matrix elements by loading the solutions onto two 2 ml Eichrom TODGA ion exchange columns stacked on top of each other[36]. To further purify the REE cut, the separation was repeated using a single 2 ml TODGA column. Separation of Sm and Nd from interfering REEs was accomplished with 0.2 cm × 25 cm quartz columns with AG50W-X8 (NH_4^+ form, with a pH of around 7) as the stationary phase and 0.2 M alpha-hydroxyisobutyric acid (pH adjusted to 4.6) as the fluid phase. The Sm and Nd cuts were passed twice over this column at the University of Chicago and were then sent to LLNL. The Nd was further purified at LLNL using 0.2 M alpha-hydroxyisobutyric acid adjusted to a pH of 4.40 on pressurized quartz glass columns loaded with AG50W-X8 (NH_4^+ form) resin. Neodymium was separated from the alpha-hydroxyisobutyric acid using 2 ml columns loaded with AG50W-X8 (200-400 mesh) resin using water, 2 M HCl, and 6 M HCl. The yields of the chemical procedure were determined by ICP-MS on small aliquots of the processed Nd and Sm cuts and ranged between 62% and 95% for Nd (with a mean yield of 80%) and 56% and 98% for Sm (with a mean yield of 75%). The variable yields do not have any noticeable influence on the measured Nd and Sm isotopic compositions. This is indicated both by the fact that several samples processed multiple times displayed variable yields, but had very homogeneous isotopic compositions, and that the terrestrial rock standards passed through the chemistry have indistinguishable compositions from the unprocessed standard. These observations further suggest that either the exponential law is well-suited to correct any yield-related induced mass-dependent isotope variations, or that the sample loss is associated with processes that do not induce mass-dependent fractionation effects, for example, pipetting of the samples on the columns or the loss of dry sample material from the beakers by static effects. The latter erratic losses seem to be the most likely explanation for the variable yields, which vary in a non-systematic way within a chemical campaign and among multiple digestions of the same meteorites. The procedural blanks associated with Nd and Sm isotope composition measurements were 50 pg and 12 pg respectively, and thus contributed negligibly (<0.03% of total analyte) to the isotope compositions of the samples, requiring no corrections to be made.

Procedures of Nd and Sm isotope measurement by TIMS. The Nd isotope compositions were analysed using a ThermoScientific Triton thermal ionization mass spectrometer (TIMS) at LLNL. Neodymium was loaded on zone-refined Re filaments in 2 M HCl and analysed as Nd^+ using a second Re ionization filament. Isotope ratios were measured using a two-mass-step procedure that calculates $^{142}Nd/^{144}Nd$ and $^{148}Nd/^{144}Nd$ ratios dynamically, while measuring the other Nd isotopes statically following a modified version of previously established procedures[17]. The cup configuration of lines 1 and 2 are: L3 = ^{142}Nd, L2 = ^{143}Nd, L1 = ^{144}Nd, C = ^{145}Nd, H1 = ^{146}Nd, H2 = ^{148}Nd, H3 = ^{149}Sm and H4 = ^{150}Nd, and L3 = ^{140}Ce, L2 = ^{141}Pr, L1 = ^{142}Nd, C = ^{143}Nd, H1 = ^{144}Nd, H2 = ^{146}Nd, H3 = ^{147}Sm and H4 = ^{148}Nd, respectively. Individual mass spectrometer runs consisted of 540 ratios of 8 s integrations. The dynamic $^{142}Nd/^{144}Nd$ ratio is calculated from $^{142}Nd/^{144}Nd$ measured in cycle 2 normalized to $^{146}Nd/^{144}Nd$ measured in cycle 1, whereas the dynamic $^{148}Nd/^{144}Nd$ ratio is calculated from the $^{148}Nd/^{146}Nd$ ratio measured in cycle 1 normalized to $^{146}Nd/^{144}Nd$ measured in cycle 2. The $^{143}Nd/^{144}Nd$ ratio is calculated from the average of the 1,080 ratios of data collected in cycles 1 and 2. The $^{145}Nd/^{144}Nd$ ratio represents the average of 540 ratios collected in cycle 1. Most samples were run at least twice from the same filaments. Signal sizes varied from $^{144}Nd = 3.2 \times 10^{-11}$ A to 5.4×10^{-11} A, with most averaging in excess of 4.3×10^{-11} A. Fractionation was corrected by assuming $^{146}Nd/^{144}Nd = 0.7219$ using the exponential law. The Nd isotope data were acquired in three measurement campaigns that were separated by a cup exchange and maintenance work on the Triton. To avoid any bias that might have been introduced by these events, the data obtained in each of the campaigns were normalized to the mean JNdi-1 composition measured in the respective campaign (see Supplementary Information). The external reproducibility of the standard (2 s.d.) for $^{142}Nd/^{144}Nd$, $^{145}Nd/^{144}Nd$, $^{148}Nd/^{144}Nd$ and $^{150}Nd/^{144}Nd$ are: 5 p.p.m., 9 p.p.m., 3 p.p.m. and 24 p.p.m. in campaign 1; 6 p.p.m., 6 p.p.m., 7 p.p.m. and 24 p.p.m. in campaign 2; and 8 p.p.m., 13 p.p.m., 15 p.p.m. and 31 p.p.m. in campaign 3. Table 1 presents the average values of multiple measurements from the same filament. The associated uncertainties represent the external reproducibility (2 s.d.) of the standard during that campaign, or the uncertainty of the sample measurements (2 s.e.), which were larger than the external reproducibility of the standard (3 p.p.m.) for some of the $^{148}Nd/^{144}Nd$ sample runs in campaign 1. Interferences from Ce and Sm are monitored at ^{140}Ce and ^{149}Sm and are presented in Supplementary Table 1.

Samarium was loaded in 2 M HCl onto a zone-refined Re filament and analysed as Sm^+ using double Re filaments. All Sm isotopes, along with the interferences from Nd (measured as ^{146}Nd) were measured statically for 200 ratios of 8 s integration each. Instrument fractionation was corrected by assuming $^{147}Sm/^{152}Sm = 0.56803$ using the exponential law. The cup configuration for Sm isotope composition measurements is: L4 = ^{144}Sm, L3 = ^{146}Nd, L2 = ^{147}Sm, L1 = ^{148}Sm, C = ^{149}Sm, H1 = ^{150}Sm, H2 = ^{152}Sm, H3 = ^{154}Sm and H4 = ^{155}Gd. Sample measurements consisted of one to three static runs from the same filament, depending on the amount of Sm available, and were obtained at $(1–2) \times 10^{-11}$ A ^{149}Sm. The data were acquired in three campaigns and are given in the Supplementary Information. Samarium isotope anomalies were calculated relative to the mean composition of the AMES Sm standard analysed in each campaign (see Supplementary Information). The external reproducibility of the standard for $^{144}Sm/^{152}Sm$, $^{148}Sm/^{152}Sm$, $^{149}Sm/^{152}Sm$, $^{150}Sm/^{152}Sm$ and $^{154}Sm/^{152}Sm$ are: 22 p.p.m., 12 p.p.m., 14 p.p.m., 12 p.p.m. and 18 p.p.m. in campaign 1; 43 p.p.m., 10 p.p.m., 10 p.p.m., 18 p.p.m. and 13 p.p.m. in campaign 2; and 38 p.p.m., 10 p.p.m., 12 p.p.m., 13 p.p.m. and 11 p.p.m. in campaign 3. Table 1 presents average

values of the multiple measurements run from the same filament, and the reported uncertainties are 2 s.d. of the standard.

The Nd and Sm concentrations were determined using a ThermoScientific TIMS in static mode. Measurements consisted of 200 cycles with 8 s integration time each. Concentration data and $^{147}Sm/^{144}Nd$ ratios are given in Supplementary Table 3. Note that the nucleosynthetic anomalies measured here have no noticeable effect on the accuracy and precision of the Sm and Nd concentration measurement (the minimum variation in the Sm and Nd isotopic compositions that would be required to shift the $^{147}Sm/^{144}Nd$ ratios beyond uncertainty are 270 μ^iSm and 560 μ^iNd units, respectively; and thus substantially larger than the deviations we observed).

Isotopic mass balance calculations between CAIs and Allende. CAIs found in carbonaceous chondrites are considered to be the oldest surviving objects to have formed in the solar nebula, presumably by condensation from nebular gas. They often exhibit isotopic anomalies that are substantially different from their chondrite host rocks[16,18,22,23,37], strongly suggesting that they are not genetically related to the reservoir from which the other chondrite components (namely chondrules and matrix) originated. The Nd and Sm isotopic composition of bulk carbonaceous chondrites is thus most likely to be influenced by CAIs, especially since the (light) REEs in these objects are enriched relative to the host rocks (for example, up to around 20× for CAIs from the CV (Vigarano-like) chondrite group, up to around 100× for CAIs from the CM (Mighei-like) chondrite group).

Indeed, our measurements imply that CAI material exert a strong control on the Nd and Sm isotope composition of bulk carbonaceous chondrites, because our Allende data (as well as literature data of carbonaceous chondrites) are displaced towards the CAI composition in μ^iNd versus μ^jNd, μ^iNd versus μ^jSm and μ^iSm versus μ^jSm (with *i* and *j* representing different isotopes of the Nd and Sm diagrams (Figs 2, 3; Extended Data Fig. 3).

To quantify the effect of CAIs on the Allende composition and characterize the composition of the CAI-free carbonaceous chondrite source reservoir we performed an isotopic mass balance calculation. For Nd this has the form

$$\mathrm{Nd_{Allende}} = X\mathrm{Nd_{source}} + (1-X)\mathrm{Nd_{CAI}} \quad (1)$$

where $Nd_{Allende}$ is the concentration of Nd in Allende, which is given by the sum of Nd in the carbonaceous chondrite source reservoir (Nd_{source}) and the Nd contributed by the CAIs (Nd_{CAI}) and *X* is the fraction of non-CAI material in Allende.

For the isotopic composition we can likewise write

$$\mu^i\mathrm{Nd_{Allende}Nd_{Allende}} = X\mu^i\mathrm{Nd_{source}Nd_{source}} + (1-X)\mu^i\mathrm{Nd_{CAI}Nd_{CAI}} \quad (2)$$

Using the isotopic compositions measured for Allende (this study), Allende CAIs (the mean value of 11 CAIs reported in ref. 22) and 3 wt% CAIs in Allende[38], and mean Nd concentrations of 0.967 p.p.m. and 14 p.p.m. for Allende and Allende CAIs[31], we can solve for the unknown concentration and isotopic composition of the CAI-free material according to

$$\mathrm{Nd_{source}} = \frac{\mathrm{Nd_{Allende}} - (1-X)\mathrm{Nd_{CAI}}}{X} \quad (3)$$

and

$$\mu^i\mathrm{Nd_{source}} = \frac{\mu^i\mathrm{Nd_{Allende}Nd_{Allende}} - (1-X)\mu^i\mathrm{Nd_{CAI}Nd_{CAI}}}{\mathrm{Nd_{Allende}} - (1-X)\mathrm{Nd_{CAI}}} \quad (4)$$

The uncertainty in $\mu^i Nd_{source}$ is mainly determined by the uncertainties in the measured isotopic compositions of Allende and the CAIs and was calculated by propagating them according to

$$\sigma^2_{\mu^i\mathrm{Nd_{source}}} = \left(\frac{\partial F_{\mu^i\mathrm{Nd_{source}}}}{\partial\, ^i\mathrm{Nd_{Allende}}}\right)^2 \sigma^2_{\mu^i\mathrm{Nd_{Allende}}} + \left(\frac{\partial F_{\mu^i\mathrm{Nd_{source}}}}{\partial\, ^i\mathrm{Nd_{CAI}}}\right)^2 \sigma^2_{\mu^i\mathrm{Nd_{CAI}}} \quad (5)$$

Where *F* refers to the function given in Equation (4). Equivalent equations can be written for Sm. The mass balance calculation was performed using mean Sm concentrations of 0.313 p.p.m. and 4.54 p.p.m. for Allende and the CAIs, respectively (that is, with chondritic Sm/Nd ratios for both objects). All input parameters and the resulting composition of the carbonaceous chondrite source reservoir are also given in Extended Data Table 2.

The Nd and Sm mass balance calculations indicate that the CAI-free carbonaceous chondrite source reservoir is characterized by an s-deficit relative to the Earth and the other chondrites, in both Nd and Sm isotopes. This is consistent with information derived from other isotope systems (for example, Sr, Zr, Mo, Ru) where carbonaceous chondrites are characterized by the largest s-deficits relative to the Earth, followed by ordinary and enstatite chondrites[16,28,29,39]. We note that carbonaceous chondrite data obtained in previous studies[15,17] also plot along the mass balance mixing relation between CAIs and a CAI-free carbonaceous chondrite source. This implies that the isotopic compositions of the other carbonaceous chondrites are also influenced by CAI-like material, and that they derive from a common s-depleted reservoir. The fact that some of the other carbonaceous chondrites also plot on the mixing line close to the bulk Allende values, despite containing fewer CAIs than CV chondrites, might be due to the higher REE enrichments in these non-CV CAIs (for example, hibonites in CM chondrites) or the fact that CAI-like material is not present in the form of well-defined inclusions but could be dispersed in the matrix in the form of small dust grains that are partially altered by parent-body metamorphism. Because no Sm and Nd isotope data for non-CV carbonaceous chondrite CAIs are available, one can only speculate on whether or not these CAIs also might carry larger nucleosynthetic Sm and Nd anomalies than Allende CAIs.

In principle, the Nd and Sm isotope compositions observed in ordinary and enstatite chondrites could also be influenced by CAIs. However, petrographic and chemical investigations imply that CAI-like material in these chondrite types is extremely rare[38,40–42]; and no Sm and Nd isotope data of these objects are available. Nevertheless, the effect of CAIs on the measured bulk Nd and Sm isotope composition of enstatite and ordinary chondrites is estimated to be no larger than 2 p.p.m. for Nd and 5 p.p.m. for Sm, respectively (Extended Data Table 2). This calculation assumes that the CAI-like material in ordinary and enstatite chondrites has a maximum REE enrichment of 50 times the concentrations in the CI (Ivuna-like) group of chondrites and an isotopic composition similar to normal Allende CAIs, and that the maximum CAI abundance in these chondrites is 0.05 wt.%. Given the small effects, we have omitted any correction of our measured data. However, we note that any such correction would result in slightly larger anomalies in non-radiogenic Nd isotopes and thus a higher $\mu^{142}Nd_{s\text{-corrected}}$; that is, an even better agreement between the nucleosynthetic anomaly-corrected μ^{142}Nd values of meteorites and the accessible Earth.

CAIs exhibit isotope anomalies in Nd and Sm, but also in many other elements[16,18,22,30,37]. To explore the collateral effects of the mass balance between CAIs and Allende defined above for Nd and Sm on other isotope systems, we also applied it to Ca, Ti, Cr, Ni, Sr, Zr, Mo and Ba. The input parameters and results are given in Extended Data Table 4. Compared with the results from Nd and Sm, the isotopic compositions calculated for the CAI-free carbonaceous chondrite source reservoir for Ca, Ti, Cr, Ni, Sr, Zr, Mo and Ba do not differ greatly from the bulk Allende values (the most noticeable change is the reduction of the μ^{50}Ti anomaly from 365 ± 34 for bulk Allende to 221 ± 46 for the CAI-free component, consistent with the measured value (189 ± 6) of a CAI-free Allende sample[18]). This is explained by the fact that the chemical enrichment of these elements in the CAIs relative to the host rock are not as strong as for Nd and Sm, and that the anomalies in the CAIs and bulk Allende are less disparate than for Nd and Sm. In other words, the CAIs have less influence on the bulk Allende isotopic composition for Ca, Ti, Cr, Ni, Sr, Zr, Mo and Ba than they have for Nd and Sm. We note, however, that the calculated CAI-free Allende compositions for the Sr, Zr, and Mo isotope anomalies are fully consistent with the inferences made above from Nd and Sm—that is, the formation of the carbonaceous chondrites from a nebular reservoir that is depleted in s-process material relative to Earth.

32. Huss, G. R. Implications of isotopic anomalies and presolar grains for the formation of the formation of the Solar System. *Antarct. Meteor. Res.* **17,** 132–152 (2004).
33. Gardner-Vandy, K. G., Lauretta, D. S. & McCoy, T. J. A petrologic, thermodynamic and experimental study of brachinites: partial melt residues of an R chondrite-like precursor. *Geochim. Cosmochim. Acta* **122,** 36–57 (2013).
34. Burkhardt, C. *et al.* NWA 5363/NWA 5400 and the Earth: isotopic twins or just distant cousins? In *46th Lunar and Planetary Science Conference* abstr. 2732 (Lunar and Planetary Institute, 2015).
35. Burkhardt, C. *et al.* Hf-W mineral isochron for Ca,Al-rich inclusions: age of the solar system and the timing of core formation in planetesimals. *Geochim. Cosmochim. Acta* **72,** 6177–6197 (2008).
36. Pourmand, A., Dauphas, N. & Ireland, T. J. A novel extraction chromatography and MC-ICP-MS technique for rapid analysis of REE, Sc and Y: revising CI-chondrite and Post-Archean Australian Shale (PAAS) abundances. *Chem. Geol.* **291,** 38–54 (2012).
37. Birck, J. L. in *Geochemistry of Non-Traditional Stable Isotopes* (eds Johnson, C. M. *et al.*) 25–64 (Mineralogical Society of America, 2004).
38. Hezel, D. C., Russell, S. S., Ross, A. J. & Kearsley, A. T. Modal abundances of CAIs: implications for bulk chondrite element abundances and fractionations. *Meteorit. Planet. Sci.* **43,** 1879–1894 (2008).
39. Moynier, F. *et al.* Planetary-scale strontium isotopic heterogeneity and the age of volatile depletion of early solar system materials. *Astrophys. J.* **758,** 45 (2012).
40. Bischoff, A. & Keil, K. Al-rich objects in ordinary chondrites: related origin of carbonaceous and ordinary chondrites and their constituents. *Geochim. Cosmochim. Acta* **48,** 693–709 (1984).
41. Bischoff, A., Keil, K. & Stöffler, D. Perovskite-hibonite-spinel-bearing inclusions and Al-rich chondrules and fragments in enstatite chondrites. *Chem. Erde-Geochem.* **44,** 97–106 (1985).
42. Dauphas, N. & Pourmand, A. Thulium anomalies and rare earth element patterns in meteorites and the Earth: nebular fractionation and the nugget effect. *Geochim. Cosmochim. Acta* **163,** 234–261 (2015).
43. Nyquist, L. E. *et al.* ^{146}Sm–^{142}Nd formation interval for the lunar mantle. *Geochim. Cosmochim. Acta* **59,** 2817–2837 (1995).

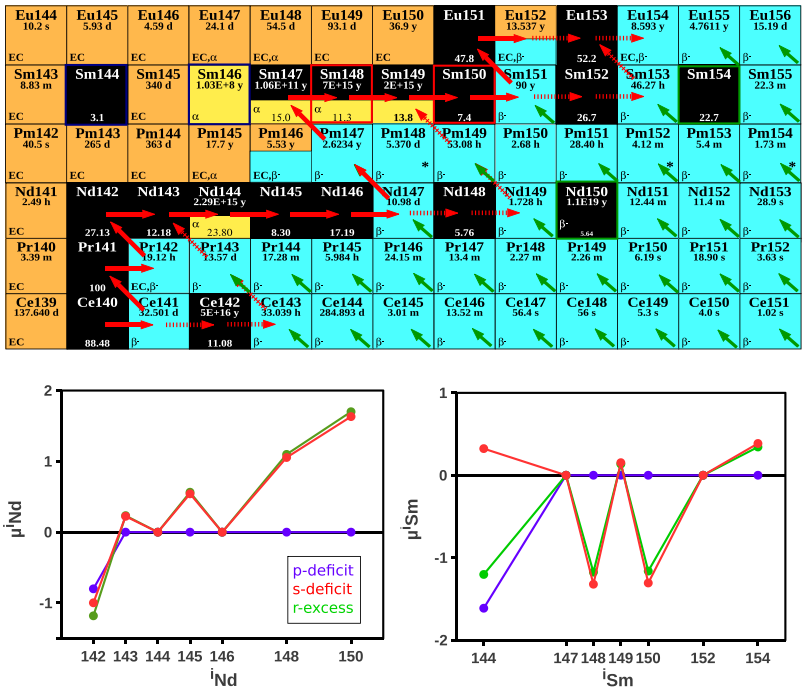

Extended Data Figure 1 | Nucleosynthetic pathways and calculated anomaly patterns for Nd and Sm. The top panel is a chart of the nuclides in the Ce–Nd–Sm–Gd mass region. Stable isotopes and their solar abundances are in black boxes on the chart, short-lived isotopes and their half-lives are in coloured boxes: blue indicates β^- unstable, orange electron capture and yellow α-decay. Solid red arrows mark the main path of s-process nucleosynthesis, the dashed red arrows mark minor s-process branches and green arrows indicate the decay path of r-process nucleosynthesis. ^{148}Sm and ^{150}Sm are produced only by the s-process, ^{150}Nd and ^{154}Sm only by the r-process and ^{144}Sm and ^{146}Sm are p-process-only isotopes. The lower panels show expected μ^iNd (left) and μ^iSm (right) anomaly patterns for a p-process deficit (purple), an s-process deficit (red) and an r-process excess (green) for internal normalization to ^{146}Nd/^{144}Nd and ^{152}Sm/^{147}Sm, calculated using stellar model abundances[27].

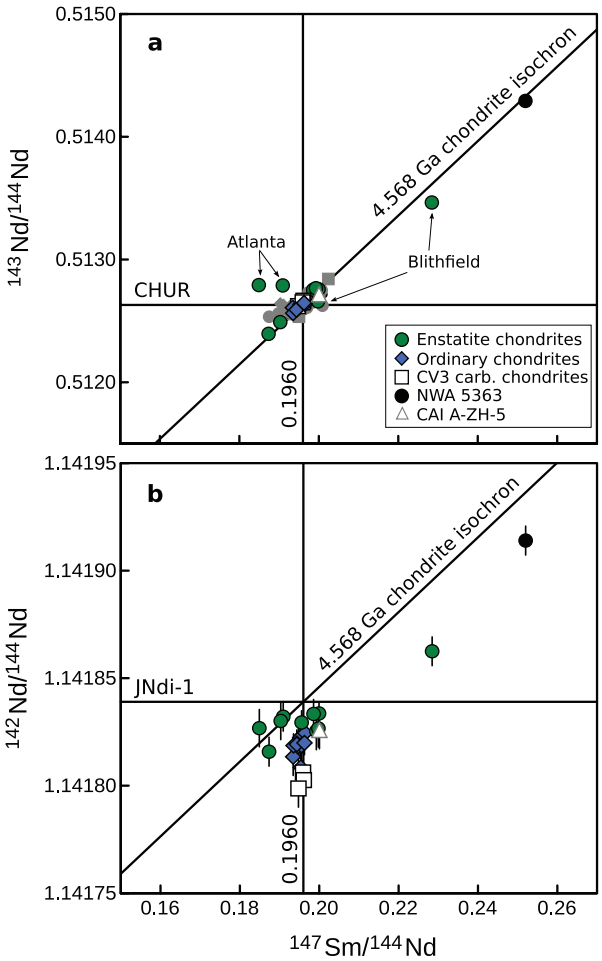

Extended Data Figure 2 | Sm/Nd isochron diagrams of measured meteorite samples. a, For $^{143}Nd/^{144}Nd$, all but the disturbed Atlanta and Blithfield chondrites cluster in a narrow range around a 4.568 Ga chondrite isochron, consistent with literature data (grey). **b**, For $^{142}Nd/^{144}Nd$, the meteorite data mostly fall below a 4.568 Ga isochron constructed through the accessible Earth value and only poorly correlate with Sm/Nd, indicating that, aside from Sm/Nd fractionation and ^{146}Sm decay, other processes are responsible for setting the $^{142}Nd/^{144}Nd$ of meteorites. Error bars represent the external reproducibility (2 s.d. of the standards run in the same measurement campaign as the samples).

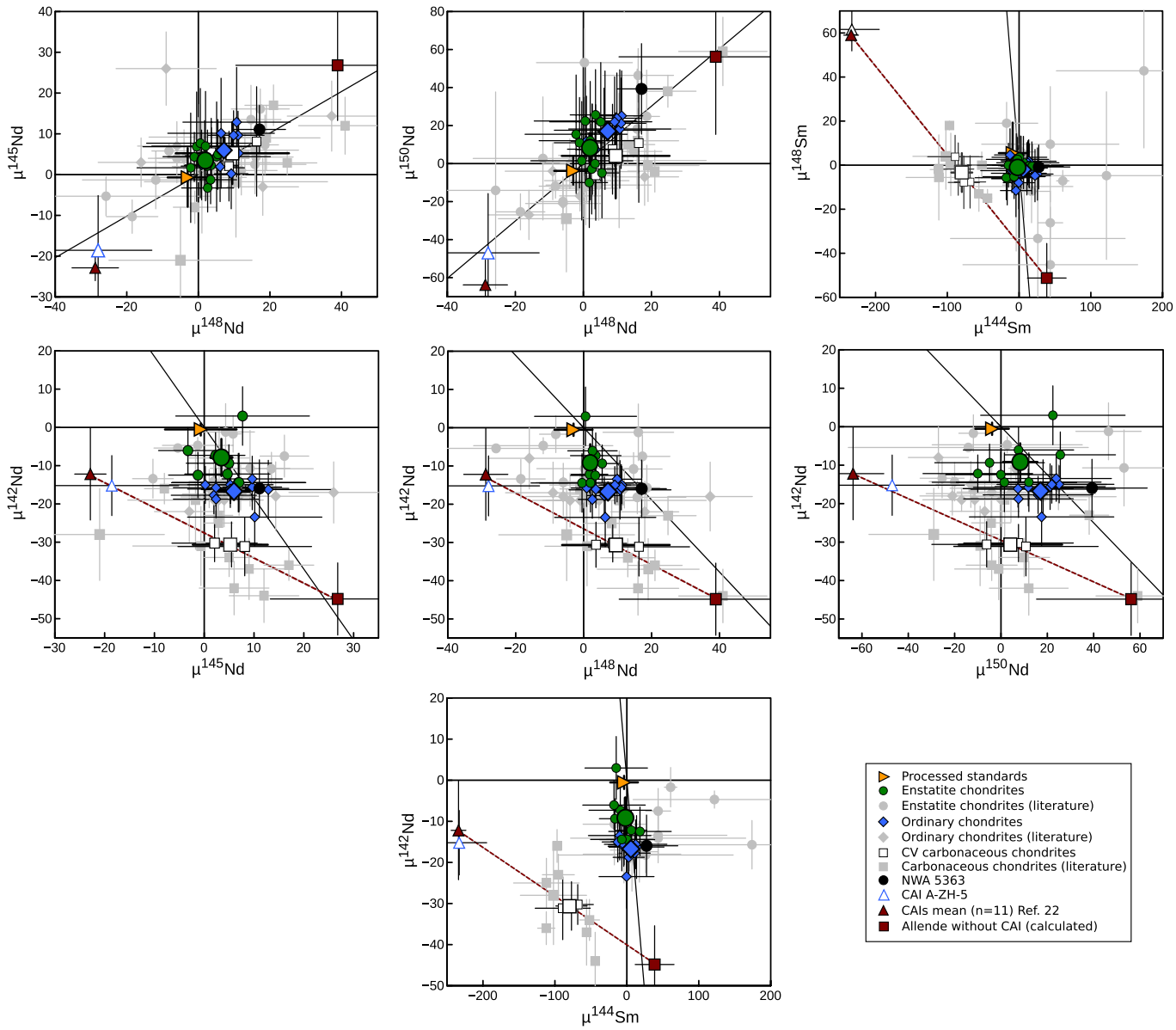

Extended Data Figure 3 | Comparison of Nd and Sm isotope data. The new data agree with literature data (in grey), but show less scatter, facilitating the calculation of more precise group averages. The error bars shown for our measurements represent external reproducibility (2 s.d. of the standards run in the same measurement campaign as the samples), whereas the uncertainties for the literature values are the 2 s.e. of the measurements. The solid lines denote mixing of the s-model prediction[27] with the terrestrial composition. The dashed lines are the mixing line between CAIs and the CAI-free carbonaceous chondrite source reservoir as calculated by isotopic mass balance.

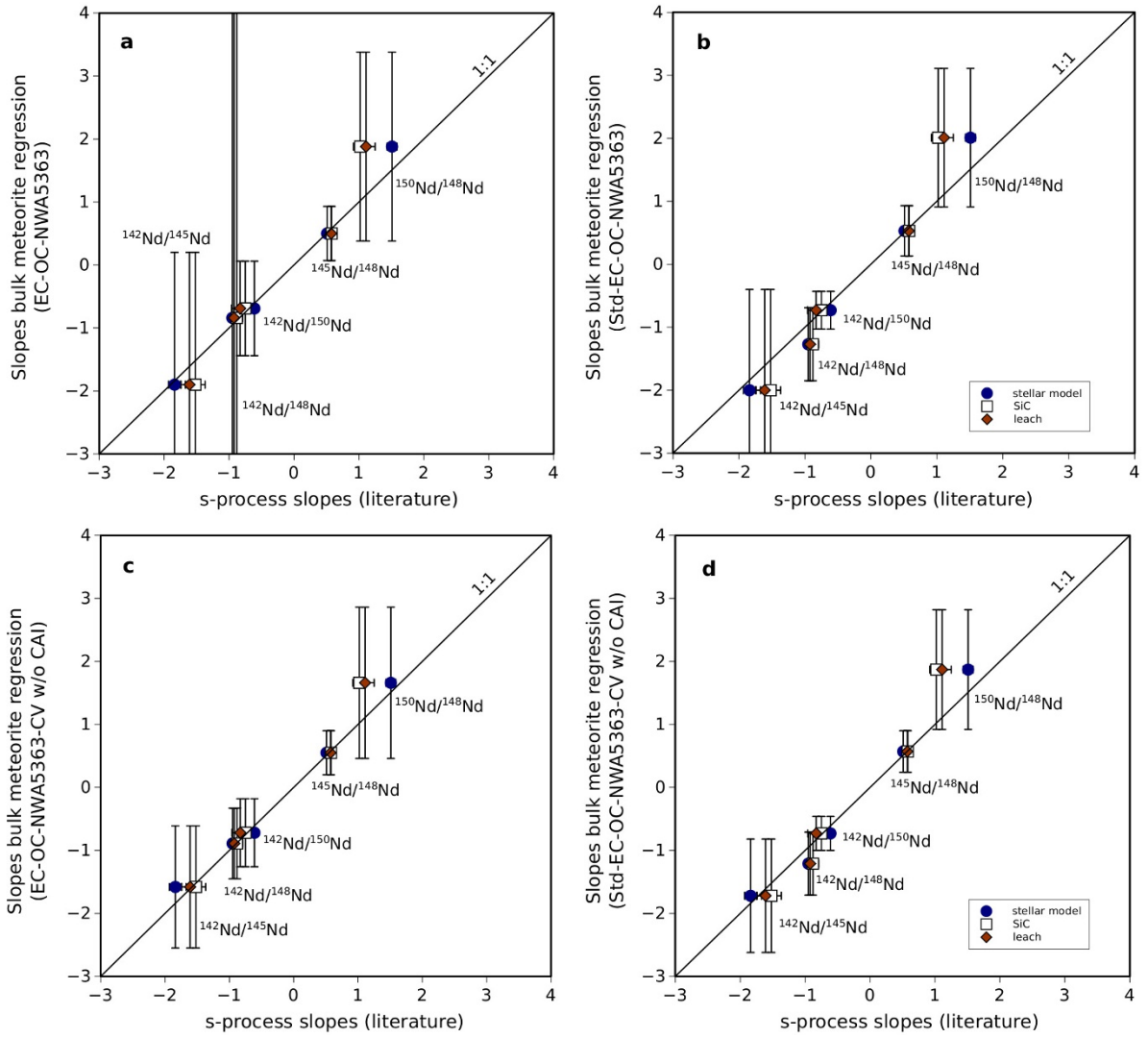

Extended Data Figure 4 | Comparison of the slopes obtained from bulk meteorite anomaly data regressions and the slopes obtained from s-process modelling, SiC grain data and chondrite leachate data. **a**, Slopes from the regression of enstatite chondrite, ordinary chondrite and NWA 5363 data. **b**, The same as **a** but including the processed standard data in the regression. **c**, Slopes from the regression of enstatite chondrite, ordinary chondrite and NWA 5363 values and calculated CAI-free Allende point ('CV w/o CAI'). **d**, The same as **c** but including the processed standard data in the regression. Within uncertainties, the slopes from the bulk meteorite regressions are indistinguishable from the slopes from the literature data[20,21,26,27], no matter which samples are used in the regressions. This implies that the Nd isotope variations in enstatite chondrites, ordinary chondrites, NWA 5363 and the CAI-free carbonaceous chondrite source are due to s-process heterogeneities. All regressions were performed using ISOPLOT. The slopes and μ^{142}Nd intercepts of the regressions are also given in Extended Data Table 3. Error bars are the 95% CI.

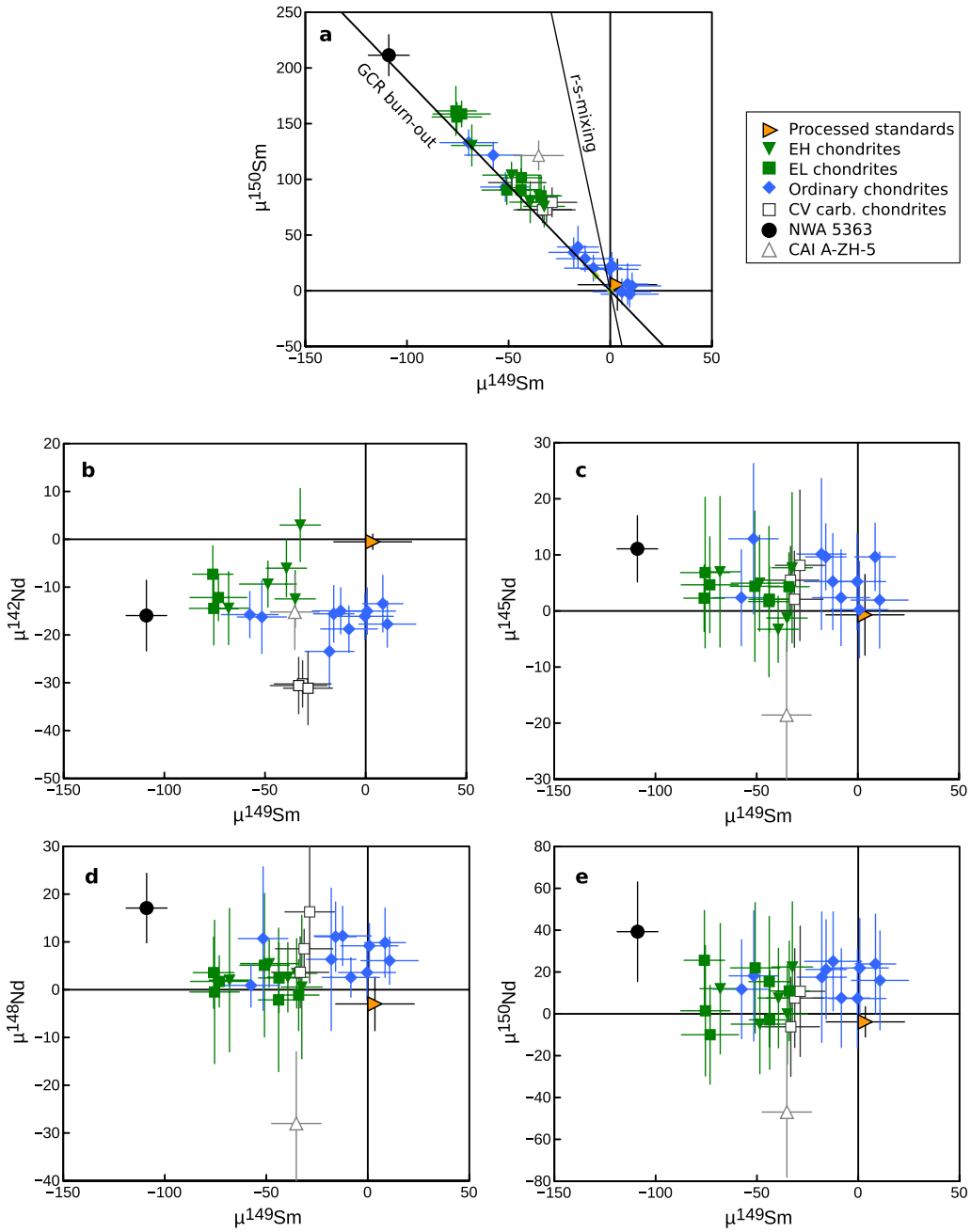

Extended Data Figure 5 | Effects of meteoroid exposure to galactic cosmic rays (GCRs) on the Sm and Nd isotope compositions. **a**, Meteorites of this study show correlated μ^{149}Sm and μ^{150}Sm anomalies that are consistent with GCR exposure. Such reactions can also alter the Nd isotope signatures of planetary materials[43]. However, given the much smaller neutron capture cross-sections of the Nd isotopes relative to ^{149}Sm, any effect of GCRs on μ^{142}Nd is <1 p.p.m. **b**–**e**, Within a given meteorite group no obvious correlations are seen in μ^{i}Nd versus μ^{149}Sm, indicating the absence of significant GCR effects on the Nd isotope data. Error bars represent the external reproducibility (2 s.d. of the standards run in the same measurement campaign as the samples).

Extended Data Table 1 | Measured and calculated $^{147}Sm/^{144}Nd$ and $\mu^{142}Nd$ values

Sample	Type	$^{147}Sm/^{144}Nd$ measured	2se	$\mu^{142}Nd$ measured	2sd	$\mu^{142}Nd$ corrected 1	2sd	$^{143}Nd/^{144}Nd$ measured	2sd	$^{147}Sm/^{144}Nd$ calculated	2sd	$\mu^{142}Nd$ corrected 2	2sd
Hvittis (1)	EL6	0.1999	0.0002	-6	5	-12	5	0.5127579	0.0000027	0.2003	0.0001	-13	5
Hvittis (2)	EL6	0.1986	0.0002	-3	6	-7	6	0.5127533	0.0000060	0.2001	0.0002	-10	6
Hvittis (3)	EL6	0.1993	0.0002	-10	8	-14	8	0.5127663	0.0000051	0.2005	0.0002	-16	8
Atlanta (1)	EL6	*0.1909*	*0.0002*	*-5*	*6*	*3*	*6*	*0.5127888*	*0.0000060*	*0.2013*	*0.0002*	*-12*	*6*
Atlanta (2)	EL6	*0.1849*	*0.0002*	*-8*	*8*	*8*	*8*	*0.5127919*	*0.0000051*	*0.2014*	*0.0002*	*-16*	*8*
Blithfield (1)	EL6	*0.2285*	*0.0002*	*22*	*6*	*-26*	*6*	*0.5134645*	*0.0000060*	*0.2236*	*0.0002*	*-19*	*6*
Blithfield (2)	EL6	*0.1998*	*0.0002*	*-9*	*8*	*-14*	*8*	*0.5126591*	*0.0000051*	*0.1970*	*0.0002*	*-10*	*8*
St. Sauveur	EH6	0.1956	0.0002	-10	5	-9	5	0.5126239	0.0000027	0.1958	0.0001	-10	5
Abee (1)	EH4	0.1874	0.0002	-19	6	-6	6	0.5123947	0.0000060	0.1883	0.0002	-7	6
Abee (2)	EH4	0.1903	0.0002	-5	8	3	8	0.5124901	0.0000051	0.1914	0.0002	1	8
Indarch (1)	EH4	0.1953	0.0002	-14	6	-12	6	0.5126219	0.0000060	0.1958	0.0002	-13	6
Indarch (2)	EH4	0.1948	0.0002	-16	8	-14	8	0.5126109	0.0000051	0.1954	0.0002	-15	8
Av. enstatite chondrites				-10.4	4.5	-9.2	4.9					-10.4	3.4
Queens Mercy	H6	0.1946	0.0002	-20	5	-18	5	0.5125971	0.0000027	0.1950	0.0001	-18	5
Allegan	H5	0.1952	0.0002	-16	5	-15	5	0.5126148	0.0000027	0.1955	0.0001	-15	5
Forest City	H5	0.1944	0.0002	-19	5	-16	5	0.5125989	0.0000027	0.1950	0.0001	-17	5
Pultusk	H5	0.1934	0.0002	-20	8	-16	8	0.5126079	0.0000051	0.1953	0.0002	-19	8
Ste. Marguerite (1)	H4	0.1955	0.0002	-16	6	-16	6	0.5126351	0.0000060	0.1962	0.0002	-17	6
Ste. Marguerite (2)	H4	0.1954	0.0002	-24	8	-23	8	0.5126355	0.0000051	0.1962	0.0002	-25	8
Bruderheim	L6	0.1935	0.0002	-19	5	-16	5	0.5125629	0.0000027	0.1938	0.0001	-16	5
Farmington (2)	L5	0.1944	0.0002	-16	6	-13	6	0.5125907	0.0000060	0.1947	0.0002	-14	6
Dhumsala	LL6	0.1965	0.0002	-14	5	-15	5	0.5126368	0.0000027	0.1963	0.0001	-15	5
Chelyabinsk	LL5	0.1963	0.0002	-18	5	-19	5	0.5126469	0.0000027	0.1966	0.0001	-19	5
Av. ordinary chondrites				-18.3	2.1	-16.7	2.0					-17.5	2.2
Allende (2)	CV3	0.1959	0.0002	-30	5	-30	5	0.5126511	0.0000027	0.1967	0.0001	-31	5
Allende (3)	CV3	0.1961	0.0002	-30	6	-31	6	0.5126644	0.0000060	0.1972	0.0002	-32	6
Allende (4)	CV3	0.1948	0.0002	-33	8	-31	8	0.5126204	0.0000051	0.1957	0.0002	-33	8
Average CV				-31.3	3.7	-30.7	1.1					-32.1	1.4
NWA 5363	Ung.	0.2520	0.0005	67.1	5.9	-16.0	7.5	0.5142920	0.0000060	0.2509	0.0002	-14.2	7.4
A-ZH-5	CAI	0.2000	0.0012	-9.2	7.6	-15.2	7.8	0.5127164	0.0000051	0.1989	0.0002	-13.5	7.7

To investigate the effect of nucleosynthetic anomalies on $\mu^{142}Nd$ with high precision, the measured $\mu^{142}Nd$ values of the meteorites first need to be corrected for ^{146}Sm decay to a constant $^{147}Sm/^{144}Nd = 0.1960$ (ref. 1) and assuming a common 4.568 Gy evolution with an initial Solar System value of $^{146}Sm/^{144}Sm = 0.00828 \pm 0.00044$ (ref. 23). This can be done either by using the measured $^{147}Sm/^{144}Nd$ values ('$\mu^{142}Nd$ corrected 1'), or the $^{147}Sm/^{144}Nd$ values are first calculated from the measured $^{143}Nd/^{144}Nd$, a chondritic $^{143}Nd/^{144}Nd = 0.512630$ (ref. 1) and the decay constant $\lambda^{147}Sm = 6.539 \times 10^{-12}$ yr^{-1}('$\mu^{142}Nd$ corrected 2'). The latter method is insensitive to recent changes in the Sm/Nd ratio (through terrestrial weathering or incomplete spike-sample equilibrium, for example) whereas the former is less model-dependent. Within uncertainties, both correction methods yield indistinguishable $\mu^{142}Nd$ values and with the exception of Abee and the radiogenic NWA 5363, these values are also indistinguishable from the measured values. For both corrections the uncertainties on the initial $^{146}Sm/^{144}Sm$, $^{147}Sm/^{144}Nd$ and the measured $\mu^{142}Nd$ were propagated, but a significant change is only observed for NWA 5363, whose decay correction (83 p.p.m.) changed the uncertainty from ± 6 p.p.m. to ± 7.5 p.p.m. Data for the Atlanta and Blithfield EL6 chondrites are excluded (italic) owing to their disturbed Sm/Nd systematics.

Extended Data Table 2 | Input parameters and the results of isotopic mass balance calculations for Nd and Sm

	Mass balance Allende – CAIs																	
	Nd (ppm)	Sm (ppm)	$^{147}Sm/^{144}Nd$	$\mu^{142}Nd$	2σ	$\mu^{145}Nd$	2σ	$\mu^{148}Nd$	2σ	$\mu^{150}Nd$	2σ	$\mu^{144}Sm$	2σ	$\mu^{148}Sm$	2σ	$\mu^{154}Sm$	2σ
CAI	14	4.54	0.1960	-12	12	-23	3	-29	7	-64	13	-234	10	59	3	-18	6
Allende	0.967	0.313	0.1960	-31	1	5	8	9	16	4	22	-80	15	-3	9	-7	13
CAI fraction = 0.03																		
Allende w/o CAI	0.564	0.183	0.1960	-45	9	27	14	39	28	56	41	39	27	-51	16	1	23

	Mass balance enstatite chondrites – CAIs																
	Nd (ppm)	Sm (ppm)	$^{147}Sm/^{144}Nd$	$\mu^{142}Nd$	2σ	$\mu^{145}Nd$	2σ	$\mu^{148}Nd$	2σ	$\mu^{150}Nd$	2σ	$\mu^{144}Sm$	2σ	$\mu^{148}Sm$	2σ	$\mu^{154}Sm$	2σ
CAI	25	8.10	0.1960	-12	12	-23	3	-29	7	-64	13	-234	10	59	3	-18	6
ECs	0.486	0.157	0.1960	-9	5	3	2	2	2	8	7	-2	8	-1	2	0	4
CAI fraction = 0.005																	
ECs w/o CAI	0.474	0.153	0.1960	-9	5	4	2	3	2	10	8	4	8	-3	2	1	4

	Mass balance ordinary chondrites – CAIs																
	Nd (ppm)	Sm (ppm)	$^{147}Sm/^{144}Nd$	$\mu^{142}Nd$	2σ	$\mu^{145}Nd$	2σ	$\mu^{148}Nd$	2σ	$\mu^{150}Nd$	2σ	$\mu^{144}Sm$	2σ	$\mu^{148}Sm$	2σ	$\mu^{154}Sm$	2σ
CAI	25	8.10	0.1960	-12	12	-23	3	-29	7	-64	13	-234	10	59	3	-18	6
OCs	0.680	0.220	0.1960	-17	2	6	3	7	3	17	5	6	7	-2	3	1	4
CAI fraction = 0.005																	
OCs w/o CAI	0.668	0.216	0.1960	-17	2	7	3	8	3	19	5	10	8	-3	3	1	5

Uncertainties for CAIs, Allende, as well as enstatite and ordinary chondrites, represent the two-sided Student's *t*-test 95% CI and were propagated throughout the mass balance calculation according to equation (5).

Extended Data Table 3 | μ^{142}Nd values corrected for nucleosynthetic anomalies

(a)	Nucleosynthetic anomaly corrected μ^{142}Nd in parts per million deviation relative to the mean measured JNdi-1 standard															
correction from intercept of	regression EC, OC, NWA								regression Std, EC, OC, NWA							
correction relation	^{145}Nd	2σ	^{148}Nd	2σ	^{150}Nd	2σ	wt. av.	2σ	^{145}Nd	2σ	^{148}Nd	2σ	^{150}Nd	2σ	wt. av.	2σ
slope rel μ^{142}Nd	-1.9	2.1	-0.84	9.8	-0.69	0.75			-2	1.6	-1.27	0.58	-0.73	0.3		
$\mu^{142}Nd_{anomaly\ corrected}$	-3	12	-9	74	-4	12	-4	10	-3	9	-6	4	-3	4	-4	3

(a) continued	Nucleosynthetic anomaly corrected μ^{142}Nd in parts per million deviation relative to the mean measured JNdi-1 standard															
correction from intercept of	regression EC, OC, NWA, CV w/o CAI								regression Std, EC, OC, NWA, CV w/o CAI							
correction relation	^{145}Nd	2σ	^{148}Nd	2σ	^{150}Nd	2σ	wt. av.	2σ	^{145}Nd	2σ	^{148}Nd	2σ	^{150}Nd	2σ	wt. av.	2σ
slope rel μ^{142}Nd	-1.58	0.97	-0.89	0.56	-0.72	0.54			-1.72	0.9	-1.21	0.5	-0.73	0.27		
$\mu^{142}Nd_{anomaly\ corrected}$	-5	7	-9	5	-4	9	-6	4	-4	6	-6	4	-3	4	-5	3

(b)	Nucleosynthetic anomaly corrected μ^{142}Nd in parts per million deviation relative to the mean measured JNdi-1 standard																					
correction using	stellar model								SiC								leachates							
correction relation	^{145}Nd	2σ	^{148}Nd	2σ	^{150}Nd	2σ	wt. av.	2σ	^{145}Nd	2σ	^{148}Nd	2σ	^{150}Nd	2σ	wt. av.	2σ	^{145}Nd	2σ	^{148}Nd	2σ	^{150}Nd	2σ	wt. av.	2σ
slope rel μ^{142}Nd	-1.84		-0.95		-0.61				-1.52		-0.88		-0.75				-1.61		-0.92		-0.83			
EC $\mu^{142}Nd_{anomaly\ corrected}$	-3	6	-7	5	-4	7	-5	3	-4	6	-8	5	-3	7	-5	3	-4	5	-7	9	-2	5	-4	3
OC $\mu^{142}Nd_{anomaly\ corrected}$	-6	6	-10	3	-6	3	-8	2	-8	5	-10	3	-4	4	-8	2	-7	5	-10	3	-3	4	-7	2
NWA $\mu^{142}Nd_{anomaly\ corrected}$	4	13	0	10	8	16	4	7	1	12	-1	10	14	19	3	7	2	12	0	10	17	21	4	8
wt. av. $\mu^{142}Nd_{anomaly\ corrected}$							-5	2							-5	2							-4	2

(a')	Nucleosynthetic anomaly corrected μ^{142}Nd in parts per million deviation relative to the mean of processed standards															
correction from intercept of	regression EC, OC, NWA								regression Std, EC, OC, NWA							
correction relation	^{145}Nd	2σ	^{148}Nd	2σ	^{150}Nd	2σ	wt. av.	2σ	^{145}Nd	2σ	^{148}Nd	2σ	^{150}Nd	2σ	wt. av.	2σ
slope rel μ^{142}Nd	-1.9	2.1	-0.84	9.8	-0.69	0.75			-2	1.6	-1.27	0.58	-0.73	0.3		
$\mu^{142}Nd_{anomaly\ corrected}$	-1	14	-6	100	-1	15	-1	12	-1	10	-2	5	0	5	-1	4

(a') continued	Nucleosynthetic anomaly corrected μ^{142}Nd in parts per million deviation relative to the mean of processed standards															
correction from intercept of	regression EC, OC, NWA, CV w/o CAI								regression Std, EC, OC, NWA, CV w/o CAI							
correction relation	^{145}Nd	2σ	^{148}Nd	2σ	^{150}Nd	2σ	wt. av.	2σ	^{145}Nd	2σ	^{148}Nd	2σ	^{150}Nd	2σ	wt. av.	2σ
slope rel μ^{142}Nd	-1.58	0.97	-0.89	0.56	-0.72	0.54			-1.72	0.9	-1.21	0.5	-0.73	0.27		
$\mu^{142}Nd_{anomaly\ corrected}$	-3	8	-6	6	0	11	-4	5	-2	7	-2	5	0	5	-1	3

(b')	Nucleosynthetic anomaly corrected μ^{142}Nd in parts per million deviation relative to the mean of processed terrestrial standards																					
correction using	stellar model								SiC								leachates							
correction relation	^{145}Nd	2σ	^{148}Nd	2σ	^{150}Nd	2σ	wt. av.	2σ	^{145}Nd	2σ	^{148}Nd	2σ	^{150}Nd	2σ	wt. av.	2σ	^{145}Nd	2σ	^{148}Nd	2σ	^{150}Nd	2σ	wt. av.	2σ
slope rel μ^{142}Nd	-1.84		-0.95		-0.61				-1.52		-0.88		-0.75				-1.61		-0.92		-0.83			
EC $\mu^{142}Nd_{anomaly\ corrected}$	-1	6	-4	5	-1	7	-2	3	-2	6	-4	5	1	7	-2	3	-2	5	-4	9	1	5	-1	3
OC $\mu^{142}Nd_{anomaly\ corrected}$	-4	6	-7	3	-3	3	-5	2	-6	5	-7	3	-1	4	-5	2	-6	5	-7	3	1	4	-4	2
NWA $\mu^{142}Nd_{anomaly\ corrected}$	6	13	4	10	11	16	6	7	3	12	2	10	17	19	6	7	4	12	3	10	20	21	7	8
wt. av. $\mu^{142}Nd_{anomaly\ corrected}$							-2	2							-2	2							-1	2

a, Correction obtained from the intercept values of regressions through the measured meteorite Nd isotope data in μ^{142}Nd versus μ^{i}Nd (where $i = 145$, 148 and 150) space (see also Fig. 3; Extended Data Fig. 4). **b**, Correction calculated from the intercepts of the measured data points and the slopes of the s-process modelling[27], isotopic compositions of SiC grains[26] and isotopic compositions of chondrite leachates[20,21] using the equation $\mu^{142}Nd_{anomaly\ corrected} = \mu^{142}Nd - \mu^{i}Nd \times slope$. EC, enstatite chondrites; OC, ordinary chondrites; NWA, NWA 5363; Std, processed terrestrial standards; CV without CAI, CAI-free Allende component as calculated from isotopic mass balance. Regressions were calculated using ISOPLOT and uncertainties of the intercept value are the 95% CI. All anomaly-corrected μ^{142}Nd values calculated for the individual meteorites are indistinguishable within uncertainty, regardless of the technique used to make the corrections (that is, using regressions through the bulk meteorite Nd data, s-process model predictions, SiC grain data or acid leachate data). The weighted averages of the anomaly-corrected μ^{142}Nd values consistently range between -6 ± 4 p.p.m. and -4 ± 2 p.p.m. relative to the mean measured JNdi-1 standard value. If all data are normalized to the mean values measured for the processed standards (**a'**, **b'**), the anomaly-corrected μ^{142}Nd values range between -4 ± 5 p.p.m. and -1 ± 2 p.p.m.

Extended Data Table 4 | Collateral effects of the isotopic mass balance between Allende and CAIs for Ca, Ti, Cr, Ni, Sr, Zr, Mo and Ba

CAI fraction = 0.03	Ca (wt%)	μ^{48}Ca	2σ
CAI	10.1	370	160
Allende	1.9	392	50
Allende w/o CAI	1.6	396	67

CAI fraction = 0.03	Ti (ppm)	μ^{46}Ti	2σ	μ^{50}Ti	2σ
CAI	6042	172	12	933	69
Allende	899	67	7	365	34
Allende w/o CAI	739	40	9	221	46

CAI fraction = 0.03	Cr (ppm)	μ^{54}Cr	2σ
CAI	997	641	90
Allende	3638	87	7
Allende w/o CAI	3720	82	7

CAI fraction = 0.03	Ni (ppm)	μ^{62}Ni	2σ	μ^{64}Ni	2σ
CAI	342	117	20	247	58
Allende	14193	11	3	31	9
Allende w/o CAI	14621	11	3	31	9

CAI fraction = 0.03	Sr (ppm)	μ^{84}Sr	2σ
CAI	66	126	11
Allende	16	63	10
Allende w/o CAI	14	54	12

CAI fraction = 0.03	Zr (ppm)	μ^{91}Zr	2σ	μ^{92}Zr	2σ	μ^{96}Zr	2σ
CAI	40	0	6	-2	14	161	31
Allende	7	2	21	-3	8	110	31
Allende w/o CAI	6	2	26	-3	10	99	38

CAI fraction = 0.03	Mo (ppm)	μ^{92}Mo	2σ	μ^{94}Mo	2σ	μ^{95}Mo	2σ	μ^{97}Mo	2σ	μ^{100}Mo	2σ
CAI	3.5	274	21	123	19	197	8	89	7	131	22
Allende	1.5	287	67	210	51	168	34	94	43	100	48
Allende w/o CAI	1.4	288	72	217	55	166	37	94	47	98	52

CAI fraction = 0.03	Ba (ppm)	μ^{130}Ba	2σ	μ^{132}Ba	2σ	μ^{135}Ba	2σ	μ^{137}Ba	2σ	μ^{138}Ba	2σ
CAI	30	-40	44	-119	74	54	6	18	5	17	9
Allende	5	63	130	13	258	26	41	19	25	9	32
Allende w/o CAI	4	87	161	44	318	20	50	19	31	8	39

Uncertainties represent the two-sided Student's *t*-test 95% CI and were propagated throughout the mass balance calculation according to equation (5). Data from refs 15–18, 22, 28–31, 37, 39 and therein.